Microwave conductivity due to impurity scattering in cuprate superconductors

Minghuan Zeng, Xiang Li, Yongjun Wang, and Shiping Feng *
Department of Physics, Beijing Normal University, Beijing 100875, China

(Received 17 July 2023; revised 24 August 2023; accepted 25 August 2023; published 7 September 2023)

Microwave surface impedance measurements on cuprate superconductors provide crucial information about the effect of impurity scattering on quasiparticle transport; however, acquiring a full understanding of the effect of impurity scattering on quasiparticle transport is still challenging. Here, starting from a homogenous electron propagator and the related microscopic octet scattering model, which are obtained within the square-lattice t-J model in the fermion-spin representation, the effect of impurity scattering on low-temperature microwave conductivity in cuprate superconductors is investigated in the self-consistent T-matrix approach. The impurity-dressed electron propagator obtained in the Fermi-arc-tip approximation of the quasiparticle excitations and scattering processes is employed to derive the electron current-current correlation function by taking into account the impurity-induced vertex correction. It is shown that the microwave conductivity spectrum is non-Drude-like, with a sharp cusplike peak extending to zero energy and a high-energy tail falling slowly with energy. Moreover, the microwave conductivity decreases with an increase in the impurity concentration or with an increase in the strength of the impurity scattering potential. In striking contrast to the domelike shape of the doping dependence of the superconducting transition temperature, the microwave conductivity exhibits a reverse domelike shape of the doping dependence. The theory also shows that the unconventional features of the microwave conductivity are generated by both the strong electron correlation and impurity scattering effects.

DOI: 10.1103/PhysRevB.108.094505

I. INTRODUCTION

For a conventional superconductor with an s-wave pairing symmetry, the impurity scattering has little effect on superconductivity [1,2]. However, cuprate superconductors are anomalously sensitive to the impurity scattering [3–6], since superconductivity involves a pairing state with the dominant d-wave symmetry [7]. In particular, the superconducting (SC) transition temperature T_c in cuprate superconductors is systematically diminished with impurities [8–15], which therefore confirms definitely that the impurity scattering has a large impact on superconductivity [3–6]. In this case, understanding the effect of the impurity scattering on superconductivity is a central issue for cuprate superconductors.

Among the striking features of the SC state in cuprate superconductivity, the physical quantity which most evidently displays the dramatic effect of the impurity scattering on superconductivity is the quasiparticle transport [3–6], which is manifested by the microwave conductivity. This microwave conductivity contains a wealth of information on the SC-state quasiparticle response and is closely associated with the superfluid density [3–6]. By virtue of systematic studies using the microwave surface impedance measurements, the low-temperature features of the SC-state quasiparticle transport in cuprate superconductors have been well established [3–6,16–20], where an agreement has emerged that the microwave conductivity is dominated mainly by thermally excited quasiparticles being scattered by impurities. In particular, as evidence of the very long-lived quasiparticle excitation deep in the SC state, the low-temperature microwave conductivity spectrum has a cusplike shape of the energy dependence [16–20]. However, it is still unclear how this microwave conductivity evolves with the impurity concentration. Moreover, experimental observations have also shown that even minor concentrations of impurities lead to changes in the temperature dependence of the magnetic field penetration depth from linear in pure systems to quadratic [21], while the ratio of the low-temperature superfluid density and effective mass of the electrons $n_s(T \to 0)/m^*$ is decreased when one increases the impurity concentration [22–24].

In the d-wave SC state of cuprate superconductors, the SC gap vanishes along the nodal direction of the electron Fermi surface (EFS) [7], and then as a natural consequence, most properties well below T_c ought to be controlled by the quasiparticle excitations around the nodal region of the EFS. In this case, the d-wave Bardeen-Cooper-Schrieffer-type (BCS-type) formalism [3–6], incorporating the effect of the impurity scattering within the self-consistent T-matrix approach, has been employed to study the effect of the impurity scattering on the microwave conductivity of cuprate superconductors [25–32], where the impurity scattering self-energy was evaluated in the nodal approximation of the quasiparticle excitations and scattering processes and then was used to calculate the electron current-current correlation function by including the contributions of the impurity-induced vertex correction and Fermi-liquid correction [26–31]. The obtained results show that both the impurity-induced vertex correction and the Fermi-liquid correction modify the microwave conductivity [26–31]. However, (i) although the contribution from

*spfeng@bnu.edu.cn

 ©2023 American Physical Society

the Fermi-liquid correction is included, these treatments suffer from ignoring the strong electron correlation effect in the homogenous part of the electron propagator [25–31], while this strong electron correlation effect also plays an important role in the SC-state quasiparticle transport; (ii) moreover, angle-resolved photoemission spectroscopy (ARPES) experiments [33–35] have shown clearly that the Fermi arcs that emerge due to the EFS reconstruction in the case of zero energy [36–43] can persist into the case for a finite binding energy, where a particularly large fraction of the spectral weight is located around the tips of the Fermi arcs. These tips of the Fermi arcs connected by the scattering wave vectors $\mathbf{q}_i$ thus construct an *octet scattering model*, and then the quasiparticle scattering with the scattering wave vectors $\mathbf{q}_i$ contributes effectively to the quasiparticle scattering processes [33–35]. In particular, this octet scattering model has been employed to give a consistent explanation of the experimental data detected from Fourier transform scanning tunneling spectroscopy [44–48] and the ARPES autocorrelation pattern observed from ARPES experiments [33–35]. These experimental results [33–48] therefore have shown clearly that the shape of the EFS has deep consequences for the various properties of cuprate superconductors, while such an aspect should also be reflected in the SC-state quasiparticle transport.

In early works [49–52], the SC mechanism and the related SC-state properties in cuprate superconductors were discussed based on the square-lattice t-J model in the fermion-spin representation, where the formation of the Fermi arcs arises from the coupling of the electrons with the spin excitations, and then the scattering wave vectors connecting the tips of the Fermi arcs construct an *octet scattering model* [52]. In our recent study [53], we started from the homogenous part of the electron propagator and the related *microscopic octet scattering model* to discuss the influence of the impurity scattering on the electronic structure of cuprate superconductors in the self-consistent T-matrix approach, where the impurity scattering self-energy is derived in the *Fermi-arc-tip approximation* of the quasiparticle excitations and scattering processes, and then the impurity-dressed electron propagator incorporates both the strong electron correlation effect and the impurity scattering effect. The obtained results [53] show that the decisive role played by the impurity scattering self-energy in the particle-hole channel is the further renormalization of the quasiparticle band structure with a reduced quasiparticle lifetime, while the impurity scattering self-energy in the particle-particle channel induces a strong deviation from the d-wave behavior of the SC gap, leading to the existence of a finite gap over the entire EFS. In this paper, we study the effect of the impurity scattering on the microwave conductivity in cuprate superconductors along this line by taking into account the impurity-induced vertex correction, where the impurity-dressed electron propagator [53] is employed to evaluate the vertex-corrected electron current-current correlation function in the self-consistent T-matrix approach, and the obtained results in the Fermi-arc-tip approximation of the quasiparticle excitations and scattering processes show that the low-temperature microwave conductivity spectrum is non-Drude-like, with a sharp cusplike peak extending to zero energy and a high-energy tail falling slowly with energy, in agreement with the corresponding experiments [16–20]. In particular, although the low-energy cusplike peak decays as $\rightarrow 1/[\omega + \text{const}]$, the overall shape of the microwave conductivity spectrum exhibits a special non-Drude-like behavior with the depicted formula that has also been used to fit the corresponding experimental data in Ref. [19]. Moreover, the microwave conductivity decreases with ascending impurity concentration or with rising strength of the impurity scattering potential. Our results therefore show that the highly unconventional features of the microwave conductivity are induced by both the strong electron correlation and the impurity scattering effects.

The remainder of this paper is organized as follows: Sec. II contains details regarding the calculation technique of the microwave conductivity in the presence of the impurity scattering. The quantitative characteristics of the impurity scattering effect on the doping and energy dependence of the microwave conductivity are presented in Sec. III, where the calculation for the microwave conductivity is performed numerically on a 120×120 lattice in momentum space, and then the obtained results show that in striking contrast to the domelike shape doping dependence of T_c, the minimum of the microwave conductivity occurs around the optimal doping and then increases in both underdoped and overdoped regimes. Finally, we give a summary in Sec. IV. In the Appendix, we present the details of the derivation of the vertex kernels of the electron current-current correlation function.

II. THEORETICAL FRAMEWORK

It was recognized shortly after the discovery of superconductivity in cuprate superconductors that the essential physics of cuprate superconductors is contained in the square-lattice t-J model [54,55],

$$H = -\sum_{ll'\sigma} t_{ll'} C^{\dagger}_{l\sigma} C_{l'\sigma} + \mu \sum_{l\sigma} C^{\dagger}_{l\sigma} C_{l\sigma} + J \sum_{l\hat{\eta}} \mathbf{S}_l \cdot \mathbf{S}_{l+\hat{\eta}}, \quad (1)$$

where $C^{\dagger}_{l\sigma}$ ($C_{l\sigma}$) creates (annihilates) a constrained electron with spin index $\sigma = \uparrow, \downarrow$ on lattice site l, $\mathbf{S}_l$ is spin operator with its components S^{x}_l, S^{y}_l, and S^{z}_l, and μ is the chemical potential. The kinetic-energy part includes the electron-hopping term $t_{ll'} = t_{\hat{\eta}} = t$ between the nearest-neighbor (NN) sites $\hat{\eta}$ and the electron-hopping term $t_{ll'} = t_{\hat{\eta}'} = t'$ between the next-nearest-neighbor sites $\hat{\eta}'$, while the magnetic-energy part is described by a Heisenberg term with the magnetic interaction J between the NN sites $\hat{\eta}$. As a qualitative discussion, the commonly used parameters in the t-J model (1) are chosen as $t/J = 2.5$ and $t'/t = 0.3$ as in our previous discussions [53]. However, when necessary to compare with the experimental data, we set $J = 1000$ K.

The basis set of the t-J model (1) is restricted by the requirement that no lattice site may be doubly occupied by electrons [56–59], i.e., $\sum_{\sigma} C^{\dagger}_{l\sigma} C_{l\sigma} \leqslant 1$. Our method employs a fermion-spin theory description of the t-J model (1) together with the on-site local constraint of no double electron occupancy [51,60], where the constrained electron operators $C_{l\uparrow}$ and $C_{l\downarrow}$ in the t-J model (1) are separated into two distinct operators as

$$C_{l\uparrow} = h^{\dagger}_{l\uparrow} S^{-}_{l}, \quad C_{l\downarrow} = h^{\dagger}_{l\downarrow} S^{+}_{l} \quad (2)$$

[with the spinful fermion operator $h_{l\sigma} = e^{-i\Phi_{l\sigma}} h_l$ that describes the charge degree of freedom of the constrained electron together with some effects of spin configuration rearrangements due to the presence of the doped hole itself (charge carrier) and the spin operator S_l that represents the spin degree of freedom of the constrained electron], and then the local constraint of no double electron occupancy is fulfilled in actual analyses.

Starting from the t-J model (1) in the fermion-spin representation (2), the kinetic-energy-driven SC mechanism has been established [49–52], where the charge carriers are held together in the d-wave pairs in the particle-particle channel due to the effective interaction, which originates directly from the kinetic energy of the t-J model (1) in the fermion-spin representation (2) by the exchange of spin excitations; then the d-wave electron pairs originating from the d-wave charge-carrier pairing state are due to the charge-spin recombination, and their condensation reveals the d-wave SC state. In these previous discussions, the homogenous electron propagator of the t-J model (1) in the SC state has been obtained explicitly in the Nambu representation as [52]

$$\begin{aligned}\tilde{G}(\mathbf{k},\omega) &= \begin{pmatrix} G(\mathbf{k},\omega), & \Im(\mathbf{k},\omega) \\ \Im^{\dagger}(\mathbf{k},\omega), & -G(\mathbf{k},-\omega)\end{pmatrix} \\ &= \frac{1}{F(\mathbf{k},\omega)}\{[\omega-\Sigma_0(\mathbf{k},\omega)]\tau_0 + \Sigma_1(\mathbf{k},\omega)\tau_1 \\ &\quad +\Sigma_2(\mathbf{k},\omega)\tau_2 + [\varepsilon_{\mathbf{k}} + \Sigma_3(\mathbf{k},\omega)]\tau_3\}, \end{aligned} \tag{3}$$

where τ_0 is the unit matrix; τ_1, τ_2, and τ_3 are Pauli matrices; $\varepsilon_{\mathbf{k}} = -4t\gamma_{\mathbf{k}} + 4t'\gamma'_{\mathbf{k}} + \mu$ is the energy dispersion in the tight-binding approximation, with $\gamma_{\mathbf{k}} = (\cos k_x + \cos k_y)/2$ and $\gamma'_{\mathbf{k}} = \cos k_x \cos k_y$; $F(\mathbf{k},\omega) = [\omega - \Sigma_0(\mathbf{k},\omega)]^2 - [\varepsilon_{\mathbf{k}} + \Sigma_3(\mathbf{k},\omega)]^2 - \Sigma_1^2(\mathbf{k},\omega) - \Sigma_2^2(\mathbf{k},\omega)$; and the homogenous self-energy has been expanded into its constituent Pauli matrix components as

$$\begin{aligned}\tilde{\Sigma}(\mathbf{k},\omega) &= \sum_{\alpha=0}^{3}\Sigma_\alpha(\mathbf{k},\omega)\tau_\alpha \\ &= \begin{pmatrix} \Sigma_0(\mathbf{k},\omega)+\Sigma_3(\mathbf{k},\omega), & \Sigma_1(\mathbf{k},\omega)-i\Sigma_2(\mathbf{k},\omega) \\ \Sigma_1(\mathbf{k},\omega)+i\Sigma_2(\mathbf{k},\omega), & \Sigma_0(\mathbf{k},\omega)-\Sigma_3(\mathbf{k},\omega)\end{pmatrix}, \end{aligned} \tag{4}$$

with $\Sigma_0(\mathbf{k},\omega)$ and $\Sigma_3(\mathbf{k},\omega)$ that being the antisymmetric and symmetric parts, respectively, of the homogenous self-energy in the particle-hole channel, while $\Sigma_1(\mathbf{k},\omega)$ and $\Sigma_2(\mathbf{k},\omega)$ are the real and imaginary parts, respectively, of the homogenous self-energy in the particle-particle channel. Moreover, these homogenous self-energies, $\Sigma_0(\mathbf{k},\omega)$, $\Sigma_1(\mathbf{k},\omega)$, $\Sigma_2(\mathbf{k},\omega)$, and $\Sigma_3(\mathbf{k},\omega)$, have been derived explicitly in Ref. [52] in terms of the full charge-spin recombination. In particular, the sharp peaks visible for temperature $T \to 0$ in $\Sigma_0(\mathbf{k},\omega)$, $\Sigma_1(\mathbf{k},\omega)$, $\Sigma_2(\mathbf{k},\omega)$, and $\Sigma_3(\mathbf{k},\omega)$ are actually a δ function, broadened by a small damping used in the numerical calculation for a finite lattice. The calculation in this paper for $\Sigma_0(\mathbf{k},\omega)$, $\Sigma_1(\mathbf{k},\omega)$, $\Sigma_2(\mathbf{k},\omega)$, and $\Sigma_3(\mathbf{k},\omega)$ is performed numerically on a 120×120 lattice in momentum space, with the infinitesimal $i0_+ \to i\Gamma$ replaced by a small damping $\Gamma = 0.05J$.

The homogenous electron spectral function can be obtained directly from the above homogenous electron propagator (3). In this case, the topology of the EFS in the pure system has been discussed in terms of the intensity map of the homogenous electron spectral function at zero energy [61–63], and the obtained results show that EFS contour is broken up into disconnected Fermi arcs located around the nodal region [36–43]; however, a large number of the low-energy electronic states are available around the tips of the Fermi arcs, and then all the anomalous properties arise from these quasiparticle excitations located around the tips of the Fermi arcs. In particular, these tips of the Fermi arcs connected by the scattering wave vectors $\mathbf{q}_i$ naturally construct an *octet scattering model*, and then the quasiparticle scattering with the scattering wave vectors $\mathbf{q}_i$ therefore contributes effectively to the quasiparticle scattering processes [44–48]. Moreover, this *octet scattering model* can persist into the case for a finite binding energy [33–35], which leads to the sharp peaks in the ARPES autocorrelation spectrum with the scattering wave vectors $\mathbf{q}_i$ being directly correlated to the regions of the highest joint density of states.

A. Impurity-dressed electron propagator

In the low-temperature limit, the framework for discussions of the impurity scattering effect is the self-consistent T-matrix approach [3–6,64–66]. The discussions of the low-temperature microwave conductivity of cuprate superconductors in this paper build on the impurity-dressed electron propagator, which is obtained from the dress of the homogenous electron propagator (3) via the impurity scattering [53], where the self-consistent T-matrix approach is employed to derive the impurity scattering self-energy in the Fermi-arc-tip approximation of the quasiparticle excitations and scattering processes. For convenience, in the following discussions of the microwave conductivity a short summary of the derivation process of the impurity-dressed electron propagator [53] is therefore given in this section.

The homogenous electron propagator in Eq. (3) is dressed due to the presence of the impurity scattering [3–6] and can be expressed explicitly as

$$\tilde{G}_{\rm I}(\mathbf{k},\omega)^{-1} = \tilde{G}(\mathbf{k},\omega)^{-1} - \tilde{\Sigma}_{\rm I}(\mathbf{k},\omega), \tag{5}$$

where, in striking similarity to the homogenous self-energy (4), the impurity scattering self-energy $\tilde{\Sigma}_{\rm I}(\mathbf{k},\omega)$ can also be expanded into its constituent Pauli matrix components as

$$\begin{aligned}\tilde{\Sigma}_{\rm I}(\mathbf{k},\omega) &= \sum_{\alpha=0}^{3}\Sigma_{{\rm I}\alpha}(\mathbf{k},\omega)\tau_\alpha \\ &= \begin{pmatrix} \Sigma_{\rm I0}(\mathbf{k},\omega)+\Sigma_{\rm I3}(\mathbf{k},\omega), & \Sigma_{\rm I1}(\mathbf{k},\omega)-i\Sigma_{\rm I2}(\mathbf{k},\omega) \\ \Sigma_{\rm I1}(\mathbf{k},\omega)+i\Sigma_{\rm I2}(\mathbf{k},\omega), & \Sigma_{\rm I0}(\mathbf{k},\omega)-\Sigma_{\rm I3}(\mathbf{k},\omega)\end{pmatrix}. \end{aligned} \tag{6}$$

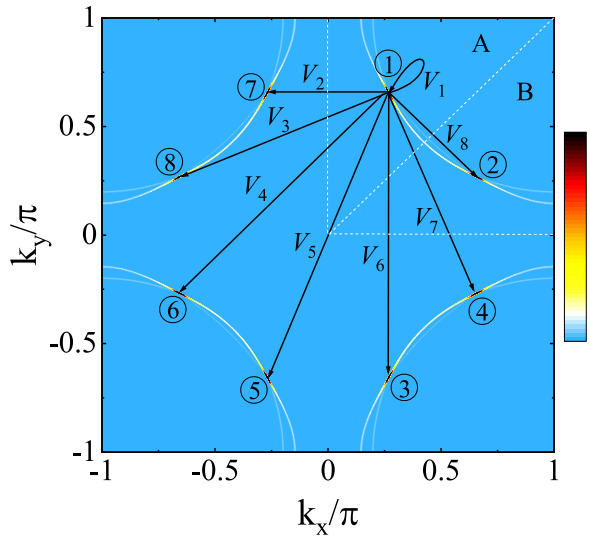

FIG. 1. The impurity scattering in the microscopic octet scattering model, where V_1 is the impurity scattering potential for the intratip scattering, V_2, V_3, V_7, and V_8 are the impurity scattering potentials for the adjacent-tip scattering, and V_4, V_5, and V_6 are the impurity scattering potentials for the opposite-tip scattering. In the d-wave superconducting state, the tips of the Fermi arcs are divided into two groups: the tips of the Fermi arcs located in the region $|k_y| > |k_x|$ (region A) and the tips of the Fermi arcs located in the region $|k_x| > |k_y|$ (region B).

The above impurity scattering self-energy together with the dressed electron propagator (5) can be analyzed in the self-consistent T-matrix approach [64–66], where $\tilde{\Sigma}_{\rm I}(\mathbf{k},\omega)$ can be derived approximately as

$$\tilde{\Sigma}_{\rm I}(\mathbf{k},\omega) = n_{\rm i} N \tilde{T}_{\mathbf{kk}}(\omega), \tag{7}$$

with the impurity concentration $n_{\rm i}$, the number of sites on a square lattice N, and the diagonal part of the T matrix $\tilde{T}_{\mathbf{kk}}(\omega)$, while the self-consistent T-matrix equation can be expressed formally by the summation of all impurity scattering processes as

$$\tilde{T}_{\mathbf{kk}'} = \frac{1}{N}\tau_3 V_{\mathbf{kk}'} + \frac{1}{N}\sum_{\mathbf{k}''} V_{\mathbf{kk}''}\tau_3 \tilde{G}_{\rm I}(\mathbf{k}'',\omega)\tilde{T}_{\mathbf{k}''\mathbf{k}'}, \tag{8}$$

where $V_{\mathbf{kk}'}$ is the momentum dependence of the impurity scattering potential. It thus shows that the initial and final momenta of an impurity scattering event must always be equal to the momentum space sited in the Brillouin zone (BZ).

However, in the microscopic octet scattering model [53] shown in Fig. 1, a particularly large fraction of the spectral weight is accommodated around eight tips of the Fermi arcs in the case of low temperatures and low energies, indicating that a large number of the quasiparticle excitations are induced only around these eight tips of the Fermi arcs. On the other hand, the strength of the impurity scattering potential $V_{\mathbf{kk}'}$ in the T-matrix equation (8) falls off quickly when the momentum shifts away from the tips of the Fermi arcs. In this case, the initial and final momenta of an impurity scattering event are always approximately equal to the momentum space sited around one of these eight tips of the Fermi arcs. In this Fermi-arc-tip approximation [53], we only need to consider three possible cases as shown in Fig. 1 for the impurity scattering potential $V_{\mathbf{kk}'}$ in the T-matrix equation (8): (i) the impurity scattering potential for the scattering process at the tip of the Fermi arc $V_{\mathbf{kk}'} = V_1$, where $\mathbf{k}$ and $\mathbf{k}'$ are located at the same tip of the Fermi arc; (ii) the impurity scattering potentials for the scattering process at the adjacent tips of the Fermi arcs $V_{\mathbf{kk}'} = V_2$, $V_{\mathbf{kk}'} = V_3$, $V_{\mathbf{kk}'} = V_7$, and $V_{\mathbf{kk}'} = V_8$, where $\mathbf{k}$ and $\mathbf{k}'$ are located at the adjacent tips of the Fermi arcs; (iii) the impurity scattering potentials for the scattering process at the opposite tips of the Fermi arcs $V_{\mathbf{kk}'} = V_4$, $V_{\mathbf{kk}'} = V_5$, and $V_{\mathbf{kk}'} = V_6$, where $\mathbf{k}$ and $\mathbf{k}'$ are located at the opposite tips of the Fermi arcs. Then the impurity scattering potential $V_{\mathbf{kk}'}$ in the self-consistent T-matrix equation (8) is reduced as an 8×8 matrix,

$$\tilde{V} = \begin{pmatrix} V_{11} & V_{12} & \cdots & V_{18} \\ V_{21} & V_{22} & \cdots & V_{28} \\ \vdots & \vdots & \ddots & \vdots \\ V_{81} & V_{82} & \cdots & V_{88} \end{pmatrix}, \tag{9}$$

where the matrix elements are given by $V_{jj} = V_1$ for $j = 1, 2, 3, \ldots, 8$; $V_{jj'} = V_{j'j} = V_2$ for $j = 1, 2, 3, 6$ with the corresponding $j' = 7, 4, 5, 8$, respectively; $V_{jj'} = V_{j'j} = V_3$ for $j = 1, 2, 3, 4$ with the corresponding $j' = 8, 7, 6, 5$, respectively; $V_{jj'} = V_{jj'} = V_4$ for $j = 1, 2, 3, 4$ with the corresponding $j' = 6, 5, 8, 7$, respectively; $V_{jj'} = V_{j'j} = V_5$ for $j = 1, 2, 3, 4$ with the corresponding $j' = 5, 6, 7, 8$, respectively; $V_{jj'} = V_{j'j} = V_6$ for $j = 1, 2, 4, 5$ with the corresponding $j' = 3, 8, 6, 7$, respectively; $V_{jj'} = V_{j'j} = V_7$ for $j = 1, 2, 5, 6$ with the corresponding $j' = 4, 3, 8, 7$, respectively; and $V_{jj'} = V_{j'j} = V_8$, for $j = 1, 3, 5, 7$ with the corresponding $j' = 2, 4, 6, 8$, respectively.

With the help of the above impurity scattering potential matrix $\tilde{V}$, the self-consistent T-matrix equation (8) is reduced as a 16×16-matrix equation around eight tips of the Fermi arcs as

$$\tilde{T}_{jj'} = \frac{1}{N}\tau_3 V_{jj'} + \frac{1}{N}\sum_{j''\mathbf{k}''} V_{jj''}[\tau_3 \tilde{G}_{\rm I}(\mathbf{k}'',\omega)]\tilde{T}_{j''j'}, \tag{10}$$

where j, j', and j'' label the tips of the Fermi arcs, the summation $\mathbf{k}''$ is restricted within the area around the tip j'' of the Fermi arc, and $\tilde{T}_{jj'}$ is now an impurity-average quantity. Then the impurity scattering self-energy $\tilde{\Sigma}_{\rm I}(\mathbf{k},\omega)$ in Eq. (7) is obtained as

$$\tilde{\Sigma}_{\rm I}(\omega) = n_{\rm i} N \tilde{T}_{jj}(\omega). \tag{11}$$

It has been shown that the diagonal propagator in Eq. (5) is symmetrical about the nodal direction, while the off-diagonal propagator is asymmetrical about the nodal direction, since the SC state has a d-wave symmetry [53]. In this case, the region of the location of the tips of the Fermi arcs has been separated into two groups: the tips of the Fermi arcs located in the region $|k_y| > |k_x|$ (region A) and the tips of the Fermi arcs located in the region $|k_x| > |k_y|$ (region B). Then the dressed electron propagator $\tilde{G}_I(\mathbf{k},\omega)$ in Eq. (5) can also be derived in regions A and B as [53]

$$\tilde{G}_{\rm I}^{(\rm A)}(\mathbf{k},\omega) = \frac{1}{F_{\rm I}^{(\rm A)}(\mathbf{k},\omega)}\{[\omega - \Sigma_0(\mathbf{k},\omega) - \Sigma_{\rm I0}(\omega)]\tau_0 + [\Sigma_1(\mathbf{k},\omega) + \Sigma_{\rm I1}^{(\rm A)}(\omega)]\tau_1$$

$$+\left[\Sigma_2(\mathbf{k},\omega)+\Sigma_{\rm I2}^{(\rm A)}(\omega)\right]\tau_2$$
$$+[\varepsilon_{\mathbf{k}}+\Sigma_3(\mathbf{k},\omega)+\Sigma_{\rm I3}(\omega)]\tau_3\Big\}, \tag{12a}$$

$$\tilde{G}_{\rm I}^{(\rm B)}(\mathbf{k},\omega)=\frac{1}{F_{\rm I}^{(\rm B)}(\mathbf{k},\omega)}\Big\{[\omega-\Sigma_0(\mathbf{k},\omega)-\Sigma_{\rm I0}(\omega)]\tau_0$$
$$+\left[\Sigma_1(\mathbf{k},\omega)+\Sigma_{\rm I1}^{(\rm B)}(\omega)\right]\tau_1$$
$$+\left[\Sigma_2(\mathbf{k},\omega)+\Sigma_{\rm I2}^{(\rm B)}(\omega)\right]\tau_2$$
$$+[\varepsilon_{\mathbf{k}}+\Sigma_3(\mathbf{k},\omega)+\Sigma_{\rm I3}(\omega)]\tau_3\Big\}, \tag{12b}$$

respectively, where $F_{\rm I}^{(\rm A)}(\mathbf{k},\omega)=[\omega-\Sigma_0(\mathbf{k},\omega)-\Sigma_{\rm I0}(\omega)]^2-[\varepsilon_{\mathbf{k}}+\Sigma_3(\mathbf{k},\omega)+\Sigma_{\rm I3}(\omega)]^2-[\Sigma_1(\mathbf{k},\omega)+\Sigma_{\rm I1}^{(\rm A)}(\omega)]^2-[\Sigma_2(\mathbf{k},\omega)+\Sigma_{\rm I2}^{(\rm A)}(\omega)]^2$ and $F_{\rm I}^{(\rm B)}(\mathbf{k},\omega)=[\omega-\Sigma_0(\mathbf{k},\omega)-\Sigma_{\rm I0}(\omega)]^2-[\varepsilon_{\mathbf{k}}+\Sigma_3(\mathbf{k},\omega)+\Sigma_{\rm I3}(\omega)]^2-[\Sigma_1(\mathbf{k},\omega)+\Sigma_{\rm I1}^{(\rm B)}(\omega)]^2-[\Sigma_2(\mathbf{k},\omega)+\Sigma_{\rm I2}^{(\rm B)}(\omega)]^2$. In the self-consistent T-matrix approach, these impurity scattering self-energies, $\Sigma_{\rm I0}^{(\rm A)}(\omega)$ $[\Sigma_{\rm I0}^{(\rm B)}(\omega)]$, $\Sigma_{\rm I1}^{(\rm A)}(\omega)$ $[\Sigma_{\rm I1}^{(\rm B)}(\omega)]$, $\Sigma_{\rm I2}^{(\rm A)}(\omega)$ $[\Sigma_{\rm I2}^{(\rm B)}(\omega)]$, and $\Sigma_{\rm I3}^{(\rm A)}(\omega)$ $[\Sigma_{\rm I3}^{(\rm B)}(\omega)]$, and the related T matrix $\tilde{T}_{jj'}^{(\rm A)}=\sum_\alpha T_{{\rm A}jj'}^{(\alpha)}\tau_\alpha$ $[\tilde{T}_{jj'}^{(\rm B)}=\sum_\alpha T_{{\rm B}jj'}^{(\alpha)}\tau_\alpha]$ with the matrix elements $T_{{\rm A}jj'}^{(\alpha)}$ $[T_{{\rm B}jj'}^{(\alpha)}]$ in Eq. (10) have been obtained in the Fermi-arc-tip approximation of the quasiparticle excitations and scattering processes and are given explicitly in Ref. [53].

With the help of the above dressed electron propagator (12) (then the dressed electron spectral function), we [53] have also discussed the influence of the impurity scattering on the electronic structure of cuprate superconductors, and the obtained results of the line shape in the quasiparticle excitation spectrum and the ARPES autocorrelation spectrum are well consistent with the corresponding experimental results [33–35,67–73].

B. Microwave conductivity

Now we turn to derive the microwave conductivity of cuprate superconductors in the presence of impurities, which is closely associated with the dressed electron propagator (12). The linear response theory allows one to obtain the microwave conductivity in terms of the Kubo formula [64],

$$\overleftrightarrow{\sigma}(\Omega,T)=-\frac{{\rm Im}\Pi^{\leftrightarrow}(\Omega)}{\Omega}, \tag{13}$$

where $\Pi^{\leftrightarrow}(\Omega)$ is the retarded electron current-current correlation function and can be expressed explicitly as

$$\overleftrightarrow{\Pi}(i\Omega_m)=-\frac{1}{N}\int_0^\beta d\tau e^{i\Omega_m\tau}\langle T_\tau \boldsymbol{J}(\tau)\boldsymbol{J}(0)\rangle, \tag{14}$$

with $\beta=1/T$, the bosonic Matsubara frequency $\Omega_m=2\pi m/\beta$, and the current density of electrons $\boldsymbol{J}$. This current density of electrons can be obtained in terms of the electron polarization operator, which is a summation over all the particles and their positions [64], and can be expressed explicitly in the fermion-spin representation (2) as $\mathbf{P}=\sum_{l\sigma}\mathbf{R}_l\hat{C}_{l\sigma}^\dagger\hat{C}_{l\sigma}=\frac{1}{2}\sum_{l\sigma}\mathbf{R}_l h_{l\sigma}h_{l\sigma}^\dagger$. Within the t-J model (1) in the fermion-spin representation (2), the current density of electrons is obtained by evaluating the time derivative of the polarization operator using Heisenberg's equation of motion as

$$\mathbf{J}=-ie[H,\mathbf{P}]=-i\frac{1}{2}et\sum_{\langle l\hat{\eta}\rangle}\hat{\eta}(h_{l+\hat{\eta}\uparrow}^\dagger h_{l\uparrow}S_l^+S_{l+\hat{\eta}}^- + h_{l+\hat{\eta}\downarrow}^\dagger h_{l\downarrow}S_l^\dagger S_{l+\hat{\eta}}^-)+i\frac{1}{2}et'\sum_{\langle l\hat{\eta}'\rangle}\hat{\eta}'(h_{l+\hat{\eta}'\uparrow}^\dagger h_{l\uparrow}S_l^+S_{l+\hat{\eta}'}^- + h_{l+\hat{\eta}'\downarrow}^\dagger h_{l\downarrow}S_l^\dagger S_{l+\hat{\eta}'}^-)$$
$$=i\frac{1}{2}et\sum_{\langle l\hat{\eta}\rangle\sigma}\hat{\eta}C_{l\sigma}^\dagger C_{l+\hat{\eta}\sigma}-i\frac{1}{2}et'\sum_{\langle l\hat{\eta}'\rangle\sigma}\hat{\eta}'C_{l\sigma}^\dagger C_{l+\hat{\eta}'\sigma}\approx -e\boldsymbol{V}_{\rm F}\sum_{\boldsymbol{k}\sigma}C_{\mathbf{k}\sigma}^\dagger C_{\mathbf{k}\sigma}, \tag{15}$$

with the electron charge e and the electron Fermi velocity $\boldsymbol{V}_{\rm F}$, which can be derived directly from the energy dispersion $\varepsilon_{\mathbf{k}}$ in the tight-binding approximation in Eq. (3) as

$$\boldsymbol{V}_{\rm F}=V_{\rm F}^{(x)}\hat{k}_x+V_{\rm F}^{(y)}\hat{k}_y=V_{\rm F}[\hat{k}_x\cos\theta_{\boldsymbol{k}_{\rm F}}+\hat{k}_y\sin\theta_{\boldsymbol{k}_{\rm F}}], \tag{16}$$

where $V_{\rm F}^{(x)}=t\sin k_{\rm F}^{(x)}-2t'\sin k_{\rm F}^{(x)}\cos k_{\rm F}^{(y)}$, $V_{\rm F}^{(y)}=t\sin k_{\rm F}^{(y)}-2t'\sin k_{\rm F}^{(y)}\cos k_{\rm F}^{(x)}$, $\cos\theta_{\boldsymbol{k}_{\rm F}}=V_{\rm F}^{(x)}/V_{\rm F}$, $\sin\theta_{\boldsymbol{k}_{\rm F}}=V_{\rm F}^{(y)}/V_{\rm F}$, and $V_{\rm F}=\sqrt{[V_{\rm F}^{(x)}]^2+[V_{\rm F}^{(y)}]^2}$. For convenience, in the following discussions of the electron current-current correlation function (14) the electron operators can be rewritten in the Nambu representation as $\Psi_{\mathbf{k}}^\dagger=(C_{\mathbf{k}\uparrow}^\dagger,C_{-\mathbf{k}\downarrow})$ and $\Psi_{\mathbf{k}}=(C_{\mathbf{k}\uparrow},C_{-\mathbf{k}\downarrow}^\dagger)^{\rm T}$, and then the current density of electrons in Eq. (15) can be rewritten in the Nambu representation as

$$\boldsymbol{J}=-e\boldsymbol{V}_{\rm F}\sum_{\boldsymbol{k}}\Psi_{\boldsymbol{k}}^\dagger\tau_0\Psi_{\boldsymbol{k}}. \tag{17}$$

With the help of the above current density of electrons (17), the impurity-induced vertex-corrected current-current correlation function (14) can be formally expressed in terms of the dressed electron propagator as

$$\overleftrightarrow{\Pi}(i\Omega_m)=\frac{1}{N}\int_0^\beta d\tau e^{i\Omega_m\tau}\overleftrightarrow{\Pi}(\tau)=(eV_{\rm F})^2\frac{1}{N}\sum_{\boldsymbol{k}}\frac{1}{\beta}\sum_{i\omega_n}\hat{\boldsymbol{k}}\,{\rm Tr}[\tilde{G}_{\rm I}(\boldsymbol{k},i\omega_n)\tilde{G}_{\rm I}(\boldsymbol{k},i\omega_n+i\Omega_m)\tilde{\Gamma}(\boldsymbol{k},i\omega_n,i\Omega_m)], \tag{18}$$

where $\omega_n=(2n+1)\pi/\beta$ is the fermionic Matsubara frequency, while the impurity-induced vertex correction in the ladder approximation can be generally expressed as [64]

$$\tilde{\Gamma}(\boldsymbol{k},i\omega_n,i\Omega_m)=\hat{\boldsymbol{k}}\tau_0+n_iN\sum_{\boldsymbol{k}''}\tilde{T}_{\boldsymbol{k}\boldsymbol{k}''}(i\omega_n+i\Omega_m)\tilde{G}_{\rm I}(\boldsymbol{k}'',i\omega_n+i\Omega_m)\tilde{\Gamma}(\boldsymbol{k}'',i\omega_n,i\Omega_m)\tilde{G}_{\rm I}(\boldsymbol{k}'',i\omega_n)\tilde{T}_{\boldsymbol{k}''\boldsymbol{k}}(i\omega_n). \tag{19}$$

Starting from the homogenous part of the d-wave BCS-type formalism, the effect of the impurity scattering on the microwave conductivity has been discussed in the self-consistent T-matrix approach by taking into account the impurity-induced vertex correction [26–31], where the vertex-corrected electron current-current correlation function and the related impurity-dressed electron propagator have been evaluated in the *nodal approximation*. In the following discussions, the vertex-corrected electron current-current correlation function is generalized from the previous case obtained in the *nodal approximation* [26–31] to the present case in the *Fermi-arc-tip approximation*, where the impurity-induced vertex correction for the electron current-current correlation function (19) can be expressed explicitly in regions A and B as

$$\tilde{\Gamma}^{(\mathrm{A})}(\boldsymbol{k}, i\omega_n, i\Omega_m) = \hat{k}_{\mathrm{F}}^{(j)}\tau_0 + \hat{k}_x^{(j)}\tilde{\Lambda}_x^{(\mathrm{A})}(i\omega_n, i\Omega_m) + \hat{k}_y^{(j)}\tilde{\Lambda}_y^{(\mathrm{A})}(i\omega_n, i\Omega_m), \quad \text{for } j \in \text{odd}, \tag{20a}$$

$$\tilde{\Gamma}^{(\mathrm{B})}(\boldsymbol{k}, i\omega_n, i\Omega_m) = \hat{k}_{\mathrm{F}}^{(j)}\tau_0 + \hat{k}_x^{(j)}\tilde{\Lambda}_x^{(\mathrm{B})}(i\omega_n, i\Omega_m) + \hat{k}_y^{(j)}\tilde{\Lambda}_y^{(\mathrm{B})}(i\omega_n, i\Omega_m), \quad \text{for } j \in \text{even}, \tag{20b}$$

respectively, while the vertex kernels $\tilde{\Lambda}_x^{(\mathrm{A})}(i\omega_n, i\Omega_m)$, $\tilde{\Lambda}_y^{(\mathrm{A})}(i\omega_n, i\Omega_m)$, $\tilde{\Lambda}_x^{(\mathrm{B})}(i\omega_n, i\Omega_m)$, and $\tilde{\Lambda}_y^{(\mathrm{B})}(i\omega_n, i\Omega_m)$ satisfy the following self-consistent equations:

$$\begin{aligned}\hat{k}_x^{(j)}\tilde{\Lambda}_x^{(\mathrm{A})}(i\omega_n, i\Omega_m) + \hat{k}_y^{(j)}\tilde{\Lambda}_y^{(\mathrm{A})}(i\omega_n, i\Omega_m) = n_i N\Bigg\{ &\sum_{\substack{\boldsymbol{k}\in\mathrm{A}\\ j''\in\text{odd}}} \tilde{T}_{jj''}(i\omega_n + i\Omega_m)\tilde{G}_{\mathrm{I}}^{(\mathrm{A})}(\boldsymbol{k}, i\omega_n + i\Omega_m)\\ &\times\big[\hat{k}_{\mathrm{F}}^{(j'')}\tau_0 + \hat{k}_x^{(j'')}\tilde{\Lambda}_x^{(\mathrm{A})}(i\omega_n, i\Omega_m) + \hat{k}_y^{(j'')}\tilde{\Lambda}_y^{(\mathrm{A})}(i\omega_n, i\Omega_m)\big]\tilde{G}_{\mathrm{I}}^{(\mathrm{A})}(\boldsymbol{k}, i\omega_n)\tilde{T}_{j''j}(i\omega_n)\\ &+ \sum_{\substack{\boldsymbol{k}\in\mathrm{B}\\ j''\in\text{even}}} \tilde{T}_{jj''}(i\omega_n + i\Omega_m)\tilde{G}_{\mathrm{I}}^{(\mathrm{B})}(\boldsymbol{k}, i\omega_n + i\Omega_m)\big[\hat{k}_{\mathrm{F}}^{(j'')}\tau_0 + \hat{k}_x^{(j'')}\tilde{\Lambda}_x^{(\mathrm{B})}(i\omega_n, i\Omega_m)\\ &+\hat{k}_y^{(j'')}\tilde{\Lambda}_y^{(\mathrm{B})}(i\omega_n, i\Omega_m)\big]\tilde{G}_{\mathrm{I}}^{(\mathrm{B})}(\boldsymbol{k}, i\omega_n)\tilde{T}_{j''j}(i\omega_n)\Bigg\}, \quad \text{for } j \in \text{odd},\end{aligned} \tag{21a}$$

$$\begin{aligned}\hat{k}_x^{(j)}\tilde{\Lambda}_x^{(\mathrm{B})}(i\omega_n, i\Omega_m) + \hat{k}_y^{(j)}\tilde{\Lambda}_y^{(\mathrm{B})}(i\omega_n, i\Omega_m) = n_i N\Bigg\{ &\sum_{\substack{\boldsymbol{k}\in\mathrm{A}\\ j''\in\text{odd}}} \tilde{T}_{jj''}(i\omega_n + i\Omega_m)\tilde{G}_{\mathrm{I}}^{(\mathrm{A})}(\boldsymbol{k}, i\omega_n + i\Omega_m)\\ &\times\big[\hat{k}_{\mathrm{F}}^{(j'')}\tau_0 + \hat{k}_x^{(j'')}\tilde{\Lambda}_x^{(\mathrm{A})}(i\omega_n, i\Omega_m) + \hat{k}_y^{(j'')}\tilde{\Lambda}_y^{(\mathrm{A})}(i\omega_n, i\Omega_m)\big]\tilde{G}_{\mathrm{I}}^{(\mathrm{A})}(\boldsymbol{k}, i\omega_n)\tilde{T}_{j''j}(i\omega_n)\\ &+ \sum_{\substack{\boldsymbol{k}\in\mathrm{B}\\ j''\in\text{even}}} \tilde{T}_{jj''}(i\omega_n + i\Omega_m)\tilde{G}_{\mathrm{I}}^{(\mathrm{B})}(\boldsymbol{k}, i\omega_n + i\Omega_m)\big[\hat{k}_{\mathrm{F}}^{(j'')}\tau_0 + \hat{k}_x^{(j'')}\tilde{\Lambda}_x^{(\mathrm{B})}(i\omega_n, i\Omega_m)\\ &+\hat{k}_y^{(j'')}\tilde{\Lambda}_y^{(\mathrm{B})}(i\omega_n, i\Omega_m)\big]\tilde{G}_{\mathrm{I}}^{(\mathrm{B})}(\boldsymbol{k}, i\omega_n)\tilde{T}_{j''j}(i\omega_n)\Bigg\}, \quad \text{for } j \in \text{even}.\end{aligned} \tag{21b}$$

Substituting the above results from Eq. (21) into Eqs. (19) and (18), the vertex-corrected electron current-current correlation function (18) now can be expressed as

$$\begin{aligned}\overleftrightarrow{\Pi}(i\Omega_m) &= \big(eV_{\mathrm{F}}^{(\mathrm{TFA})}\big)^2\frac{1}{N}\sum_{\boldsymbol{k}}\frac{1}{\beta}\sum_{i\omega_n}(\hat{k}_x + \hat{k}_y)\mathrm{Tr}\big\{\tilde{G}_{\mathrm{I}}(\boldsymbol{k}, i\omega_n)\tilde{G}_{\mathrm{I}}(\boldsymbol{k}, i\omega_n + i\Omega_m)[\hat{k}_{\mathrm{F}}\tau_0 + \hat{k}_x\tilde{\Lambda}_x(i\omega_n, i\Omega_m) + \hat{k}_y\tilde{\Lambda}_y(i\omega_n, i\Omega_m)]\big\}\\ &= \big(eV_{\mathrm{F}}^{(\mathrm{TFA})}\big)^2\sum_{j\in\text{odd}}\frac{1}{\beta}\sum_{i\omega_n}\big(\hat{k}_x^{(j)} + \hat{k}_y^{(j)}\big)\mathrm{Tr}\Bigg\{\frac{1}{N}\sum_{\boldsymbol{k}\in\mathrm{A}}\tilde{G}_{\mathrm{I}}^{(\mathrm{A})}(\boldsymbol{k}, i\omega_n)\tilde{G}_{\mathrm{I}}^{(\mathrm{A})}(\boldsymbol{k}, i\omega_n + i\Omega_m)\big[\hat{k}_{\mathrm{F}}^{(j)}\tau_0 + \hat{k}_x^{(j)}\tilde{\Lambda}_x^{(\mathrm{A})}(i\omega_n, i\Omega_m)\\ &\quad+\hat{k}_y^{(j)}\tilde{\Lambda}_y^{(\mathrm{A})}(i\omega_n, i\Omega)_m\big]\Bigg\} + \big(eV_{\mathrm{F}}^{(\mathrm{TFA})}\big)^2\sum_{j\in\text{even}}\frac{1}{\beta}\sum_{i\omega_n}\big(\hat{k}_x^{(j)} + \hat{k}_y^{(j)}\big)\mathrm{Tr}\Bigg\{\frac{1}{N}\sum_{\boldsymbol{k}\in\mathrm{B}}\tilde{G}_{\mathrm{I}}^{(\mathrm{B})}(\boldsymbol{k}, i\omega_n)\tilde{G}_{\mathrm{I}}^{(\mathrm{B})}(\boldsymbol{k}, i\omega_n + i\Omega_m)\\ &\quad\times\big[\hat{k}_{\mathrm{F}}^{(j)}\tau_0 + \hat{k}_x^{(j)}\tilde{\Lambda}_x^{(\mathrm{B})}(i\omega_n, i\Omega_m) + \hat{k}_y^{(j)}\tilde{\Lambda}_y^{(\mathrm{B})}(i\omega_n, i\Omega_m)\big]\Bigg\},\end{aligned} \tag{22}$$

with the electron Fermi velocity $V_{\mathrm{F}}^{(\mathrm{TFA})}$ around the tips of the Fermi arcs. However, in the absence of an external magnetic field, the rotational symmetry in the system is unbroken, indicating that $\Pi_{xy}(\Omega) = \Pi_{yx}(\Omega) = 0$ and $\Pi_{xx}(\Omega) = \Pi_{yy}(\Omega)$, and then the above vertex-corrected electron current-current correlation function (22) is reduced as

$$\overleftrightarrow{\Pi}(i\Omega_m) = \begin{pmatrix}\Pi_{xx}(i\Omega_m) & 0\\ 0 & \Pi_{yy}(i\Omega_m)\end{pmatrix} = \tau_0\Pi_{xx}(i\Omega_m), \tag{23}$$

where $\Pi_{xx}(i\Omega_m)$ is given by

$$\Pi_{xx}(i\Omega_m) = \left(2eV_{\rm F}^{(\rm TFA)}\right)^2 \frac{1}{\beta}\sum_{i\omega_n} J_{xx}(i\omega_n, i\omega_n + i\Omega_m), \tag{24}$$

with the kernel function

$$\begin{aligned} J_{xx}(i\omega_n, i\omega_n + i\Omega_m) = \frac{1}{N}\sum_{\alpha=0}^{3}\Big\{ &\cos^2\theta_{\rm F}^{(\rm A)}\tilde{I}_0^{(\rm A)}(\alpha, i\omega_n, i\omega_n + i\Omega_m){\rm Tr}\big[\tau_\alpha\big[\tau_0 + \tilde{\Lambda}_x^{(\rm A)}(i\omega_n, i\Omega_m)\big]\big] \\ &+ \cos^2\theta_{\rm F}^{(\rm B)}\tilde{I}_0^{(\rm B)}(\alpha, i\omega_n, i\omega_n + i\Omega_m){\rm Tr}\big[\tau_\alpha\big[\tau_0 + \tilde{\Lambda}_x^{(B)}(i\omega_n, i\Omega_m)\big]\big]\Big\}, \end{aligned} \tag{25}$$

where the functions $\tilde{I}_0^{(\rm A)}(\alpha, i\omega_n, i\omega_n + i\Omega_m)$ and $\tilde{I}_0^{(\rm B)}(\alpha, i\omega_n, i\omega_n + i\Omega_m)$ are defined as

$$\sum_{\boldsymbol{k}\in \rm A}\tilde{G}_{\rm I}^{(\rm A)}(\boldsymbol{k}, i\omega_n)\tau_\gamma\tilde{G}_{\rm I}^{(\rm A)}(\boldsymbol{k}, i\omega_n + i\Omega_m) = \sum_{\beta=0}^{3}\tilde{I}_\gamma^{(\rm A)}(\beta, i\omega_n, i\omega_n + i\Omega_m)\tau_\beta, \tag{26a}$$

$$\sum_{\boldsymbol{k}\in \rm B}\tilde{G}_{\rm I}^{(\rm B)}(\boldsymbol{k}, i\omega_n)\tau_\gamma\tilde{G}_{\rm I}^{(\rm B)}(\boldsymbol{k}, i\omega_n + i\Omega_m) = \sum_{\beta=0}^{3}\tilde{I}_\gamma^{(\rm B)}(\beta, i\omega_n, i\omega_n + i\Omega_m)\tau_\beta, \tag{26b}$$

respectively. After a quite complicated calculation, the function ${\rm Tr}[\tau_\alpha\tilde{\Lambda}_x^{(\rm A)}(\omega, \Omega)]$ in the above kernel function (25), which is a trace of the product of the vertex kernel $\tilde{\Lambda}_x^{(\rm A)}(\omega, \Omega)$ and matrix τ_α with $\alpha = 0, 1, 2, 3$ in region A of the BZ, and the function ${\rm Tr}[\tau_\alpha\tilde{\Lambda}_x^{(\rm B)}(\omega, \Omega)]$ in the above kernel function (25), which is a trace of the product of the vertex kernel $\tilde{\Lambda}_x^{(\rm B)}(\omega, \Omega)$ and matrix τ_α in region B of the BZ, can be derived straightforwardly (see the Appendix), and then the above kernel function $J_{xx}(\omega, \omega + \Omega)$ can be obtained explicitly.

On the other hand, the dressed electron propagators $\tilde{G}_{\rm I}(\boldsymbol{k}, i\omega_n)$ and $\tilde{G}_{\rm I}(\boldsymbol{k}, i\omega_n + i\Omega_m)$ are involved directly in the above kernel function $J_{xx}(i\omega_n, i\omega_n + i\Omega_m)$ in Eq. (25); then the singularity of $J_{xx}(i\omega_n, i\omega_n + i\Omega_m)$ only lies on the real axes ($\epsilon \in \mathbb{R}$) and those parallel to the real axes ($\epsilon - i\Omega_m$). In this case, the contribution for the summation of the kernel function $J_{xx}(i\omega_n, i\omega_n + i\Omega_m)$ in Eq. (24) over the fermionic Matsubara frequency $i\omega_n$ comes from the two branch cuts, $\epsilon \in \mathbb{R}$ and $\epsilon - i\Omega_m$, and then the vertex-corrected electron current-current correlation function (24) can be expressed as

$$\begin{aligned} \Pi_{xx}(i\Omega_m) = i\left(2eV_{\rm F}^{(\rm TFA)}\right)^2 \int_{-\infty}^{\infty}\frac{d\epsilon}{2\pi} n_{\rm F}(\epsilon)[&J_{xx}(\epsilon + i\delta, \epsilon + i\Omega_m) - J_{xx}(\epsilon - i\delta, \epsilon + i\Omega_m) \\ &+ J_{xx}(\epsilon - i\Omega_m, \epsilon + i\delta) - J_{xx}(\epsilon - i\Omega_m, \epsilon - i\delta)], \end{aligned} \tag{27}$$

By virtue of the analytical continuation $i\Omega_m \to \Omega + i\delta$, the above vertex-corrected electron current-current correlation function (27) can be obtained explicitly as

$$\begin{aligned} \Pi_{xx}(\Omega) = i\left(2eV_{\rm F}^{(\rm TFA)}\right)^2 \int_{-\infty}^{\infty}\frac{d\epsilon}{2\pi}\{&n_{\rm F}(\epsilon)[J_{xx}(\epsilon + i\delta, \epsilon + \Omega + i\delta) - J_{xx}(\epsilon - i\delta, \epsilon + \Omega + i\delta)] \\ &+ n_{\rm F}(\epsilon + \Omega)[J_{xx}(\epsilon - i\delta, \epsilon + \Omega + i\delta) - J_{xx}(\epsilon - i\delta, \epsilon + \Omega - i\delta)]\}, \end{aligned} \tag{28}$$

and then the microwave conductivity $\sigma^{\leftrightarrow}(\Omega, T) = \tau_0\sigma(\Omega, T)$ in Eq. (13) in the presence of impurities is obtained as

$$\sigma(\Omega) = -\frac{{\rm Im}\Pi_{xx}(\Omega)}{\Omega} = \left(2eV_{\rm F}^{(\rm TFA)}\right)^2 \int_{-\infty}^{\infty}\frac{d\epsilon}{2\pi}\frac{n_{\rm F}(\epsilon) - n_{\rm F}(\epsilon + \Omega)}{\Omega}[{\rm Re}J_{xx}(\epsilon - i\delta, \epsilon + \Omega + i\delta) - {\rm Re}J_{xx}(\epsilon + i\delta, \epsilon + \Omega + i\delta)]. \tag{29}$$

III. QUANTITATIVE CHARACTERISTICS

In the self-consistent T-matrix approach, the strength of the impurity scattering potential is an important parameter. Unless otherwise indicated, the adjacent-tip impurity scattering V_2, V_3, V_7, and V_8, and the opposite-tip impurity scattering V_4, V_5, and V_6 in the following discussions are chosen as $V_2 = 0.85V_1$, $V_3 = 0.8V_1$, $V_7 = 0.8V_1$, $V_8 = 0.9V_1$, $V_4 = 0.7V_1$, $V_5 = 0.65V_1$, and $V_6 = 0.75V_1$, respectively, as in the previous discussions of the influence of the impurity scattering on the electronic structure [53], while the strength of the intratip impurity scattering V_1 is chosen as $V_1 = V_{\rm scale}\tan(\frac{\pi}{2}d)$ with $V_{\rm scale} = 58J$ and the adjustable parameter d of the impurity scattering potential strength, where the case of $d \sim 0$ [then $\tan(\frac{\pi}{2}d) \sim 0$] corresponds to the case $V_j \sim 0$ with $j = 1, 2, 3, \ldots, 8$ in the Born limit, while the case of $d \sim 1$ [then $\tan(\frac{\pi}{2}d) \sim \infty$] corresponds to the case $V_j \sim \infty$ in the unitary limit.

We are now ready to discuss the effect of the impurity scattering on the microwave conductivity in cuprate superconductors. We have performed a calculation for the microwave conductivity $\sigma(\omega, T)$ in Eq. (29), and the results of the microwave conductivity $\sigma(\omega, T)$ as a function of energy at the doping concentration $\delta = 0.15$ for temperatures $T =$

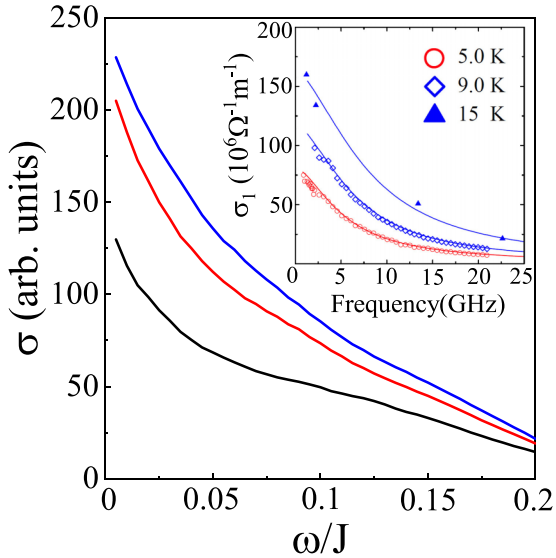

FIG. 2. The microwave conductivity as a function of energy at the doping concentration $\delta = 0.15$ for temperatures $T = 0.005J \sim 5$ K (black line), $T = 0.009J \sim 9$ K (red line), and $T = 0.015J \sim 15$ K (blue line) together with the impurity concentration $n_i = 0.0025$ and parameter of the impurity scattering potential strength $d = 0.05$. Inset: the corresponding experimental result of the microwave conductivity observed in $YBa_2Cu_3O_{6.993}$ taken from Ref. [20].

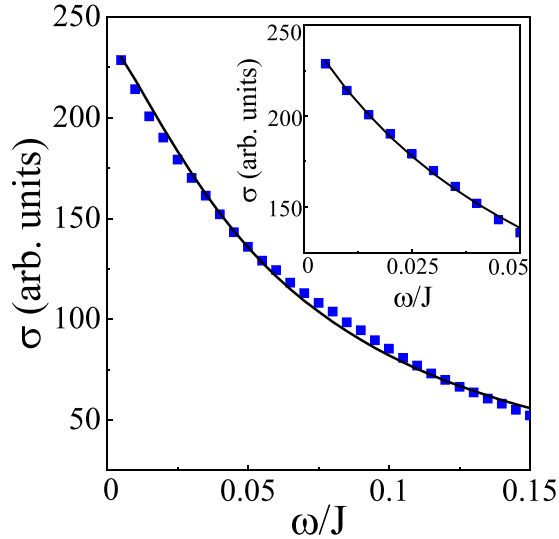

FIG. 3. The numerical fit (black line) with Eq. (30). The blue squares are the result of the microwave conductivity with $T = 0.015J \sim 15$ K taken from Fig. 2. Inset: the numerical fit (black line) with the fit form $\sigma(\omega, T) = A_0/[\omega + B_0]$, where $A_0 = 15.676$ and $B_0 = 0.063$. The blue squares are the result of the low-energy microwave conductivity with $T = 0.015J \sim 15$ K taken from Fig. 2.

$0.005J \sim 5$ K (black line), $T = 0.009J \sim 9$ K (red line), and $T = 0.015J \sim 15$ K (blue line) together with the impurity concentration $n_i = 0.0025$ and the parameter of the impurity scattering potential strength $d = 0.05$ are plotted in Fig. 2 in comparison with the corresponding experimental results of the microwave conductivity observed on the cuprate superconductor [20] $YBa_2Cu_3O_{6.993}$ (inset). The results in Fig. 2 therefore show clearly that the energy dependence of the low-temperature microwave conductivity in a cuprate superconductor [16–20] is qualitatively reproduced, where the highly unconventional features of the low-temperature microwave conductivity spectrum can be summarized as follows: (i) A sharp cusplike peak develops at the low-energy limit, (ii) the low-temperature microwave conductivity spectrum is non-Drude-like, and (iii) a high-energy tail falls slowly with the increase in energy. To see this non-Drude-like behavior in the low-temperature microwave conductivity spectrum more clearly, the results of the low-temperature microwave conductivity spectra shown in Fig. 2 have been numerically fitted in terms of the fit form

$$\sigma(\omega, T) = \frac{\sigma_0}{1 + (\omega/C_0 T)^y}, \tag{30}$$

as has been done in experiments [19], and the fit result at the temperature $T = 0.015J \sim 15$ K is plotted in Fig. 3 (black line), with the fit parameters $\sigma_0 = 238.073$, $C_0 = 4.145$, and $y = 1.333$. For a better understanding, we have also fitted the low-energy part of the microwave conductivity spectrum alone with the fit form $\sigma(\omega, T) = A_0/[\omega + B_0]$, and the numerically fitted result at the same temperature $T = 0.015J \sim 15$ K is also plotted in the inset of Fig. 3, with the fit parameters $A_0 = 15.676$ and $B_0 = 0.063$. These fit results in Fig. 3 thus indicate clearly that although the lower-energy cusplike peak in Fig. 2 decays as $\to 1/[\omega + B_0]$, the overall shape of the low-temperature microwave conductivity spectrum in Fig. 2 exhibits a special non-Drude-like behavior, which can be well fitted by the formula in Eq. (30), in agreement with the corresponding experimental observations [19,20]. More specifically, in comparison with other fit results at the temperatures $T = 0.005J \sim 5$ K and $T = 0.009J \sim 9$ K, we also find that the fit parameter y in the fit form (30) is almost independent of temperature and remains relatively constant, taking an average value of $y = 1.333$. This anticipated value of the fit parameter $y = 1.333$ is not too far from the corresponding value of $y = 1.45(\pm 0.06)$, which has been employed in Ref. [19] to fit the corresponding experimental data with the same fit formula (30). The qualitative agreement between the present theoretical results and experimental data therefore also shows that the kinetic-energy-driven superconductivity, incorporating the effect of the impurity scattering within the framework of the self-consistent T-matrix theory, can give a consistent description of the low-temperature microwave conductivity spectrum found in microwave surface impedance measurements on cuprate superconductors [16–20].

As a natural consequence of the doped Mott insulator, the microwave conductivity in cuprate superconductors evolves with doping. In Fig. 4, we plot the result of $\sigma(\omega, T)$ (black line) as a function of doping with $T = 0.002J$ for energy $\omega = 0.0025J$ together with $n_i = 0.0025$ and $d = 0.05$. For a comparison, the corresponding result [50–52] of T_c obtained within the framework of the kinetic-energy-driven superconductivity is also shown in Fig. 4 (red line). Apparently, in striking contrast to the domelike shape of the doping dependence of T_c, the microwave conductivity exhibits a reverse domelike shape of the doping dependence, where $\sigma(\omega, T)$ is a decreasing function of the doping concentration, and the

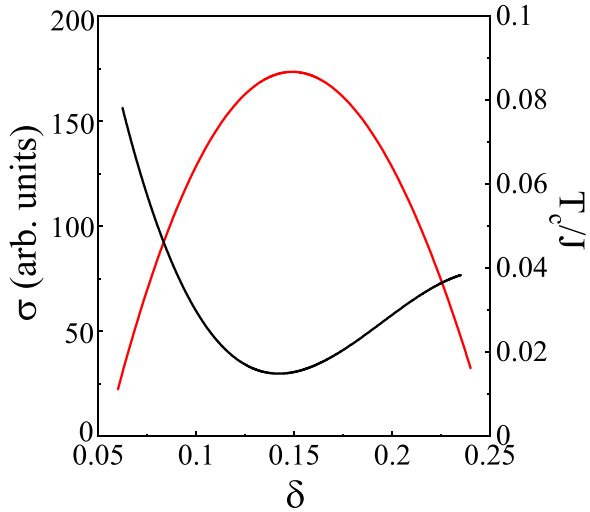

FIG. 4. The microwave conductivity (black line) as a function of doping with $T = 0.002J$ for $\omega = 0.0025J$ together with $n_i = 0.0025$ and $d = 0.05$. The red line is the corresponding result of T_c.

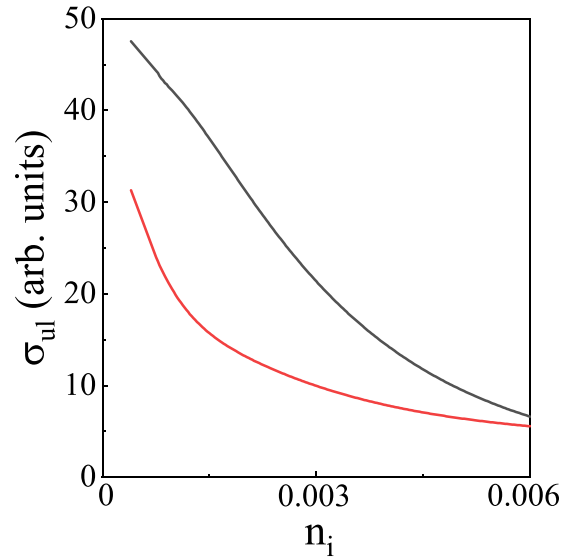

FIG. 5. The microwave conductivity in the universal limit as a function of the impurity concentration at $\delta = 0.15$ with $T = 0.002J$ for $d = 0.05$ (black line) and $d = 0.5$ (red line).

system is thought to be in the underdoped regime. The system is at around the *optimal doping*, where $\sigma(\omega, T)$ reaches its minimum. However, with the further increase in the doping concentration, $\sigma(\omega, T)$ increases in the overdoped regime. This reverse domelike shape of the doping dependence of the microwave conductivity at low energies and low temperatures is also qualitatively consistent with the microwave conductivity $\sigma_{\rm ul} \propto 1/\bar{\Delta}$ in the universal limit of $\omega \to 0$ and $T \to 0$, since the SC gap parameter $\bar{\Delta}$ obtained within the framework of the kinetic-energy-driven superconductivity [50–52] has a similar domelike shape of the doping dependence.

For a further understanding of the intrinsic effect of the impurity scattering on the SC-state quasiparticle transport in cuprate superconductors, we now turn to discuss the evolution of the microwave conductivity with the impurity concentration in the case of the universal limit. The microwave conductivity $\sigma_{\rm ul}$ in the universal limit can be obtained directly from the energy and temperature dependence of the microwave conductivity (29) in the zero-temperature ($T \to 0$) and zero-energy ($\Omega \to 0$) limits as

$$\begin{aligned}\sigma_{\rm ul} &= \lim_{\substack{\Omega\to 0\\ T\to 0}} \sigma_{xz}(\Omega)\\ &= \frac{\left(2eV_{\rm F}^{\rm (TFA)}\right)^2}{2\pi} \lim_{\epsilon\to 0}[{\rm Re}J_{xx}(\epsilon - i\delta, \epsilon + i\delta)\\ &\quad -{\rm Re}J_{xx}(\epsilon + i\delta, \epsilon + i\delta)]. \end{aligned} \tag{31}$$

In this case, we have made a series of calculations for $\sigma_{\rm ul}$ at different impurity concentrations and different strengths of the impurity scattering potential, and the results of $\sigma_{\rm ul}$ as a function of the impurity concentration n_i at $\delta = 0.15$ for $d = 0.05$ (black line) and $d = 0.5$ (red line) are plotted in Fig. 5, where the main features can be summarized as follows: (i) For a given set of impurity scattering potential strengths, the microwave conductivity gradually decreases with the increase in the impurity concentration; (ii) for a given impurity concentration, the microwave conductivity decreases when the strength of the impurity scattering potential is increased. In other words, the crucial role played by the impurity scattering is the further reduction of the microwave conductivity.

In the present theoretical framework, the effect of the strong electron correlation on the microwave conductivity is reflected in the homogenous part of the electron propagator (then the homogenous self-energy), while the effect of the impurity scattering on the microwave conductivity is reflected both in the impurity-dressed electron propagator (then the impurity scattering self-energy) and the impurity-induced vertex correction to the electron current-current correlation function. In other words, the microwave conductivity is further renormalized by the impurity-induced vertex correction. To understand this renormalization of the microwave conductivity from the impurity-induced vertex correction, the microwave conductivity in the case of the universal limit in Eq. (31) can be rewritten as

$$\sigma_{\rm ul} = \beta_{\rm vc}\sigma_{\rm ul}^{(0)}, \tag{32}$$

where the characteristic factor $\beta_{\rm vc}$ is the impurity-induced vertex correction to the universal bare result of the microwave conductivity $\sigma_{\rm ul}^{(0)}$, while this $\sigma_{\rm ul}^{(0)}$ can be reduced directly from $\sigma_{\rm ul}$ in Eq. (31) by ignoring the impurity-induced vertex correction as

$$\begin{aligned}\sigma_{\rm ul}^{(0)} &= \frac{\left(2eV_{\rm F}^{\rm (TFA)}\right)^2}{\pi} \lim_{\epsilon\to 0} \sum_{\mu={\rm A,B}} \Theta^{(\mu)}(\theta_{\rm F})\\ &\quad \times {\rm Re}\big[\tilde{I}_0^{(\mu)}(0, \epsilon - i\delta, \epsilon + i\delta) - \tilde{I}_0^{(\mu)}(0, \epsilon + i\delta, \epsilon + i\delta)\big], \end{aligned} \tag{33}$$

with the function

$$\Theta^{(\mu)}(\theta_{\rm F}) = \begin{cases} \cos\theta_{\rm F}^{\rm (A)}, & \text{for } \mu = {\rm A}\\ \cos\theta_{\rm F}^{\rm (B)}, & \text{for } \mu = {\rm B}. \end{cases}$$

In Fig. 6, we plot the characteristic factor $\beta_{\rm vc} - 1$ as a function of the impurity concentration n_i at $\delta = 0.15$ for $d = 0.05$

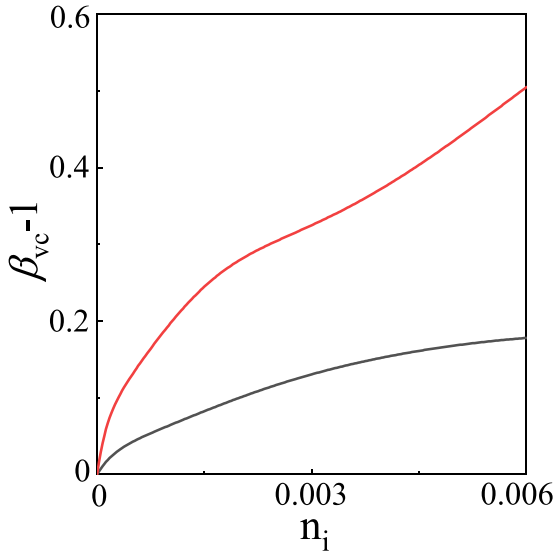

FIG. 6. The characteristic factor of the impurity-induced vertex correction as a function of the impurity concentration at $\delta = 0.15$ for $d = 0.05$ (black line) and $d = 0.5$ (red line).

(black line) and $d = 0.5$ (red line), where for a given set of the impurity scattering potential strength, the characteristic factor monotonically *increases* as the impurity concentration is increased. On the other hand, for a given impurity concentration, $\beta_{vc} - 1$*increases* with the increase in the strength of the impurity scattering potential. It thus shows clearly that the impurity-induced vertex correction is quite significant in the renormalization of the microwave conductivity [26–32], and then all the effects of the strong electron correlation, the impurity-scattering self-energy, and the impurity-induced vertex correction lead to the highly unconventional behaviors in the microwave conductivity of cuprate superconductors [16–20].

IV. SUMMARY

Starting from the homogenous electron propagator and the related microscopic octet scattering model, which are obtained within the framework of the kinetic-energy-driven superconductivity, we have rederived the impurity-dressed electron propagator in the self-consistent T-matrix approach, where the impurity scattering self-energy is evaluated in the Fermi-arc-tip approximation of the quasiparticle excitations and scattering processes, and then the impurity-dressed electron propagator incorporates both the strong electron correlation and impurity scattering effects. By virtue of this impurity-dressed electron propagator, we then have investigated the effect of the impurity scattering on the low-temperature microwave conductivity of cuprate superconductors, where the electron current-current correlation function is derived by taking into account the impurity-induced vertex correction. The obtained results show clearly that the low-temperature microwave conductivity spectrum is non-Drude-like, with a sharp cusplike peak extending to zero energy and a high-energy tail falling slowly with energy, in agreement with the corresponding experimental observations [16–20]. In particular, although the low-energy cusplike peak decays as $\rightarrow A_0/[\omega + B_0]$, the overall shape of the low-temperature microwave conductivity spectrum exhibits a special non-Drude-like behavior and can be well fitted by the formula $\sigma(\omega, T) = \sigma_0/[1 + (\omega/C_0T)^{\mathrm{y}}]$ with the relatively temperature-independent constant y. Moreover, the low-temperature microwave conductivity decreases with the increase in the impurity concentration or with the increase in the strength of the impurity scattering potential. Our results therefore indicate that the highly unconventional features of the microwave conductivity in cuprate superconductors arise from both the strong electron correlation and impurity scattering effects. The theory also predicts a reverse domelike shape of the doping dependence of the microwave conductivity, which is in a striking contrast to the domelike shape of the doping dependence of T_c and therefore should be verified by further experiments.

ACKNOWLEDGMENTS

This work is supported by the National Key Research and Development Program of China under Grant No. 2021YFA1401803 and the National Natural Science Foundation of China under Grants No. 12247116, No. 11974051, and No. 12274036.

APPENDIX: DERIVATION OF VERTEX KERNELS OF THE ELECTRON CURRENT-CURRENT CORRELATION FUNCTION

Starting from the homogenous part of the d-wave BCS-type formalism, the electron current-current correlation function has been discussed by taking into account the impurity-induced vertex correction [26–32], where the T-matrix approach has been employed to derive the vertex kernels of the electron current-current correlation function in the nodal approximation. In this Appendix, we generalize these previous calculations [26–32] for the vertex kernels of the electron current-current correlation function in the nodal approximation to the present case in the Fermi-arc-tip approximation. In the microscopic octet scattering model shown in Fig. 1, the tips of the Fermi arcs labeled by odd numbers are located in region A of the BZ, where $|k_y| > |k_x|$, while the tips of the Fermi arcs labeled by even numbers are located in region B of the BZ, where $|k_x| > |k_y|$. For convenience in the following discussions, $j = 1$ in Eq. (21a) is chosen in region A of the BZ, and $j = 2$ in Eq. (21b) is chosen in region B of the BZ; then the trace of the product between the self-consistent equation (21a) and the unit vector $\hat{k}_x^{(1)}$ in region A and the trace

of the product between the self-consistent equation (21b) and the unit vector $\hat{k}_x^{(2)}$ in region B can be obtained as

$$\mathrm{Tr}\big[\tau_0\tilde{\Lambda}_x^{(\mathrm{A})}(\omega,\Omega)\big] = \frac{n_iN}{\cos^2\theta_{\mathrm{F}}^{(\mathrm{A})}}\sum_{\boldsymbol{k}\in\mathrm{A}}\mathrm{Tr}\left[\tilde{G}_{\mathrm{I}}^{(\mathrm{A})}(\boldsymbol{k},\omega)\sum_{j''\in\mathrm{odd}}\hat{k}_x^{(1)}\cdot\hat{k}_{\mathrm{F}}^{(j'')}\tilde{T}_{j''1}(\omega)\tilde{T}_{1j''}(\omega+\Omega)\tilde{G}_{\mathrm{I}}^{(\mathrm{A})}(\boldsymbol{k},\omega+\Omega)\big[\tau_0+\tilde{\Lambda}_x^{(\mathrm{A})}(\omega,\Omega)\big]\right]$$
$$+\frac{n_iN}{\cos^2\theta_{\mathrm{F}}^{(\mathrm{A})}}\sum_{\boldsymbol{k}\in\mathrm{B}}\mathrm{Tr}\left[\tilde{G}_{\mathrm{I}}^{(\mathrm{B})}(\boldsymbol{k},\omega)\sum_{j''\in\mathrm{even}}\hat{k}_x^{(1)}\cdot\hat{k}_{\mathrm{F}}^{(j'')}\tilde{T}_{j''1}(\omega)\tilde{T}_{1j''}(\omega+\Omega)\tilde{G}_{\mathrm{I}}^{(\mathrm{B})}(\boldsymbol{k},\omega+\Omega)\big[\tau_0+\tilde{\Lambda}_x^{(\mathrm{B})}(\omega,\Omega)\big]\right], \tag{A1a}$$

$$\mathrm{Tr}\big[\tau_0\tilde{\Lambda}_x^{(\mathrm{B})}(\omega,\Omega)\big] = \frac{n_iN}{\cos^2\theta_{\mathrm{F}}^{(\mathrm{B})}}\sum_{\boldsymbol{k}\in\mathrm{A}}\mathrm{Tr}\left[\tilde{G}_{\mathrm{I}}^{(\mathrm{A})}(\boldsymbol{k},\omega)\sum_{j''\in\mathrm{odd}}\hat{k}_x^{(2)}\cdot\hat{k}_{\mathrm{F}}^{(j'')}\tilde{T}_{j''2}(\omega)\tilde{T}_{2j''}(\omega+\Omega)\tilde{G}_{\mathrm{I}}^{(\mathrm{A})}(\boldsymbol{k},\omega+\Omega)\big[\tau_0+\tilde{\Lambda}_x^{(\mathrm{A})}(\omega,\Omega)\big]\right]$$
$$+\frac{n_iN}{\cos^2\theta_{\mathrm{F}}^{(\mathrm{B})}}\sum_{\boldsymbol{k}\in\mathrm{B}}\mathrm{Tr}\left[\tilde{G}_{\mathrm{I}}^{(\mathrm{B})}(\boldsymbol{k},\omega)\sum_{j''\in\mathrm{even}}\hat{k}_x^{(2)}\cdot\hat{k}_{\mathrm{F}}^{(j'')}\tilde{T}_{j''2}(\omega)\tilde{T}_{2j''}(\omega+\Omega)\tilde{G}_{\mathrm{I}}^{(\mathrm{B})}(\boldsymbol{k},\omega+\Omega)\big[\tau_0+\tilde{\Lambda}_x^{(\mathrm{B})}(\omega,\Omega)\big]\right], \tag{A1b}$$

respectively, where the Fermi velocity unit vectors $\hat{k}_{\mathrm{F}}^{(j)}$ with $j=1,2,3,\ldots,8$ at the tips of the Fermi arc are defined as follows: $\hat{k}_{\mathrm{F}}^{(1)}=\hat{k}_x\cos\theta_{\mathrm{F}}+\hat{k}_y\sin\theta_{\mathrm{F}}$, $\hat{k}_{\mathrm{F}}^{(2)}=\hat{k}_x\sin\theta_{\mathrm{F}}+\hat{k}_y\cos\theta_{\mathrm{F}}$, $\hat{k}_{\mathrm{F}}^{(3)}=\hat{k}_x\cos\theta_{\mathrm{F}}-\hat{k}_y\sin\theta_{\mathrm{F}}$, $\hat{k}_{\mathrm{F}}^{(4)}=\hat{k}_x\sin\theta_{\mathrm{F}}-\hat{k}_y\cos\theta_{\mathrm{F}}$, $\hat{k}_{\mathrm{F}}^{(5)}=-\hat{k}_x\cos\theta_{\mathrm{F}}-\hat{k}_y\sin\theta_{\mathrm{F}}$, $\hat{k}_{\mathrm{F}}^{(6)}=-\hat{k}_x\sin\theta_{\mathrm{F}}-\hat{k}_y\cos\theta_{\mathrm{F}}$, $\hat{k}_{\mathrm{F}}^{(7)}=-\hat{k}_x\cos\theta_{\mathrm{F}}+\hat{k}_y\sin\theta_{\mathrm{F}}$, and $\hat{k}_{\mathrm{F}}^{(8)}=-\hat{k}_x\sin\theta_{\mathrm{F}}+\hat{k}_y\cos\theta_{\mathrm{F}}$. In particular, it is easy to verify the relations

$$\frac{n_iN}{\cos^2\theta_{\mathrm{F}}}\sum_{j''\in\mathrm{odd}}\hat{k}_x^{(1)}\cdot\hat{k}_{\mathrm{F}}^{(j'')}\tilde{T}_{j''1}(\omega)\tilde{T}_{1j''}(\omega+\Omega) = n_iN[\tilde{T}_{11}(\omega)\tilde{T}_{11}(\omega+\Omega)+\tilde{T}_{31}(\omega)\tilde{T}_{13}(\omega+\Omega)$$
$$-\tilde{T}_{51}(\omega)\tilde{T}_{15}(\omega+\Omega)-\tilde{T}_{71}(\omega)\tilde{T}_{17}(\omega+\Omega)], \tag{A2a}$$

$$\frac{n_iN}{\cos^2\theta_{\mathrm{F}}}\sum_{j''\in\mathrm{even}}\hat{k}_x^{(1)}\cdot\hat{k}_{\mathrm{F}}^{(j'')}\tilde{T}_{j''1}(\omega)\tilde{T}_{1j''}(\omega+\Omega) = \tan\theta_{\mathrm{F}}n_iN[\tilde{T}_{21}(\omega)\tilde{T}_{12}(\omega+\Omega)+\tilde{T}_{41}(\omega)\tilde{T}_{14}(\omega+\Omega)$$
$$-\tilde{T}_{61}(\omega)\tilde{T}_{16}(\omega+\Omega)-\tilde{T}_{81}(\omega)\tilde{T}_{18}(\omega+\Omega)], \tag{A2b}$$

$$\frac{n_iN}{\sin^2\theta_{\mathrm{F}}}\sum_{j''\in\mathrm{odd}}\hat{k}_x^{(2)}\cdot\hat{k}_{\mathrm{F}}^{(j'')}\tilde{T}_{j''2}(\omega)\tilde{T}_{2j''}(\omega+\Omega) = \cot\theta_{\mathrm{F}}n_iN[\tilde{T}_{12}(\omega)\tilde{T}_{21}(\omega+\Omega)+\tilde{T}_{32}(\omega)\tilde{T}_{23}(\omega+\Omega)$$
$$-\tilde{T}_{52}(\omega)\tilde{T}_{25}(\omega+\Omega)-\tilde{T}_{72}(\omega)\tilde{T}_{27}(\omega+\Omega)], \tag{A2c}$$

$$\frac{n_iN}{\sin^2\theta_{\mathrm{F}}}\sum_{j''\in\mathrm{even}}\hat{k}_x^{(2)}\cdot\hat{k}_{\mathrm{F}}^{(j'')}\tilde{T}_{j''2}(\omega)\tilde{T}_{2j''}(\omega+\Omega) = n_iN[\tilde{T}_{22}(\omega)\tilde{T}_{22}(\omega+\Omega)+\tilde{T}_{42}(\omega)\tilde{T}_{24}(\omega+\Omega)$$
$$-\tilde{T}_{62}(\omega)\tilde{T}_{26}(\omega+\Omega)-\tilde{T}_{82}(\omega)\tilde{T}_{28}(\omega+\Omega)], \tag{A2d}$$

in regions A and B of the BZ, respectively, with the T matrix

$$T^{(\alpha)}(\omega) = \begin{pmatrix} T_{\mathrm{AA}}^{(\alpha)}(\omega) & T_{\mathrm{AB}}^{(\alpha)}(\omega) \\ T_{\mathrm{BA}}^{(\alpha)}(\omega) & T_{\mathrm{BB}}^{(\alpha)}(\omega)\end{pmatrix}, \tag{A3}$$

where the matrices $T_{\mu\nu}^{(\alpha)}(\omega)$ $(\mu,\nu=\mathrm{A},\mathrm{B})$ with the corresponding matrix elements have been given explicitly in Ref. [53]. Moreover, a general formalism is satisfied by $\tilde{T}_{jn}(\omega)\tilde{T}_{nj}(\omega+\Omega)$ as

$$\tilde{T}_{jn}(\omega)\tilde{T}_{nj}(\omega+\Omega) = \sum_{\alpha,\beta=0}^{3}\tau_\alpha T_{jn}^{(\alpha)}(\omega)\tau_\beta T_{nj}^{(\beta)}(\omega+\Omega) = \sum_{\alpha,\beta,\gamma=0}^{3} i\bar{\epsilon}_{\alpha\beta\gamma}T_{jn}^{(\alpha)}(\omega)T_{nj}^{(\beta)}(\omega+\Omega)\tau_\gamma, \tag{A4}$$

with $i\bar{\epsilon}_{\alpha\beta\gamma}$ that is defined as

$$i\bar{\epsilon}_{\alpha\beta\gamma} = \delta_{\alpha\beta}\delta_{\gamma0}+(1-\delta_{\alpha0})\delta_{\beta0}\delta_{\gamma\alpha}+\delta_{\alpha0}(1-\delta_{\beta0})\delta_{\gamma\beta}+i\epsilon_{\alpha\beta\gamma}, \tag{A5}$$

where $\epsilon_{\alpha\beta\gamma}$ is the Levi-Civita tensor, and then $i\bar{\epsilon}_{\alpha\beta\gamma}$ satisfies the following identities: $\tau_\alpha\tau_\beta = \sum_\gamma i\bar{\epsilon}_{\alpha\beta\gamma}\tau_\gamma$ and $i\bar{\epsilon}_{\alpha\beta\gamma} = i\bar{\epsilon}_{\gamma\alpha\beta}$. With the help of the above general formalism (A4), the relations in Eq. (A2) can be derived as

$$\frac{n_i N}{\cos^2\theta_{\rm F}}\sum_{j''\in{\rm odd}}\hat{k}_x^{(1)}\cdot\hat{k}_{\rm F}^{(j'')}\tilde{T}_{j''1}(\omega)\tilde{T}_{1j''}(\omega+\Omega)=\sum_\gamma C_{\rm A1}^{(x)}(\gamma)\tau_\gamma, \tag{A6a}$$

$$C_{\rm A1}^{(x)}(\gamma)=n_iN\sum_{\alpha,\beta=0}^{3}i\bar{\epsilon}_{\alpha\beta\gamma}\big[T_{11}^{(\alpha)}(\omega)T_{11}^{(\beta)}(\omega+\Omega)+T_{31}^{(\alpha)}(\omega)T_{13}^{(\beta)}(\omega+\Omega)-T_{51}^{(\alpha)}(\omega)T_{15}^{(\beta)}(\omega+\Omega)-T_{71}^{(\alpha)}(\omega)T_{17}^{(\beta)}(\omega+\Omega)\big], \tag{A6b}$$

$$\frac{n_i N}{\sin^2\theta_{\rm F}}\sum_{j''\in{\rm odd}}\hat{k}_x^{(2)}\cdot\hat{k}_{\rm F}^{(j'')}\tilde{T}_{j''1}(\omega)\tilde{T}_{1j''}(\omega+\Omega)=\sum_\gamma C_{\rm A2}^{(x)}(\gamma)\tau_\gamma, \tag{A6c}$$

$$C_{\rm A2}^{(x)}(\gamma)=\cot\theta_{\rm F}n_iN\sum_{\alpha,\beta=0}^{3}i\bar{\epsilon}_{\alpha\beta\gamma}\big[T_{12}^{(\alpha)}(\omega)T_{21}^{(\beta)}(\omega+\Omega)+T_{32}^{(\alpha)}(\omega)T_{23}^{(\beta)}(\omega+\Omega)-T_{52}^{(\alpha)}(\omega)T_{25}^{(\beta)}(\omega+\Omega)-T_{72}^{(\alpha)}(\omega)T_{27}^{(\beta)}(\omega+\Omega)\big], \tag{A6d}$$

$$\frac{n_i N}{\cos^2\theta_{\rm F}}\sum_{j''\in{\rm even}}\hat{k}_x^{(1)}\cdot\hat{k}_{\rm F}^{(j'')}\tilde{T}_{j''1}(\omega)\tilde{T}_{1j''}(\omega+\Omega)=\sum_\gamma C_{\rm B1}^{(x)}(\gamma)\tau_\gamma, \tag{A6e}$$

$$C_{\rm B1}^{(x)}(\gamma)=n_iN\tan\theta_{\rm F}\sum_{\alpha,\beta=0}^{3}i\bar{\epsilon}_{\alpha\beta\gamma}\big[T_{21}^{(\alpha)}(\omega)T_{12}^{(\beta)}(\omega+\Omega)+T_{41}^{(\alpha)}(\omega)T_{14}^{(\beta)}(\omega+\Omega)-T_{61}^{(\alpha)}(\omega)T_{16}^{(\beta)}(\omega+\Omega)-T_{81}^{(\alpha)}(\omega)T_{18}^{(\beta)}(\omega+\Omega)\big], \tag{A6f}$$

$$\frac{n_i N}{\sin^2\theta_{\rm F}}\sum_{j''\in{\rm even}}\hat{k}_x^{(2)}\cdot\hat{k}_{\rm F}^{(j'')}\tilde{T}_{j''2}(\omega)\tilde{T}_{2j''}(\omega+\Omega)=\sum_\gamma C_{\rm B2}^{(x)}(\gamma)\tau_\gamma, \tag{A6g}$$

$$C_{\rm B2}^{(x)}(\gamma)=n_iN\sum_{\alpha,\beta=0}^{3}i\bar{\epsilon}_{\alpha\beta\gamma}\big[T_{22}^{(\alpha)}(\omega)T_{22}^{(\beta)}(\omega+\Omega)+T_{42}^{(\alpha)}(\omega)T_{24}^{(\beta)}(\omega+\Omega)-T_{62}^{(\alpha)}(\omega)T_{26}^{(\beta)}(\omega+\Omega)-T_{82}^{(\alpha)}(\omega)T_{28}^{(\beta)}(\omega+\Omega)\big]. \tag{A6h}$$

Substituting the above results from Eq. (A6) into Eqs. (A1a) and (A1b), $\mathrm{Tr}[\tau_0\tilde{\Lambda}_x^{(\rm A)}(\omega,\Omega)]$ and $\mathrm{Tr}[\tau_0\tilde{\Lambda}_x^{(\rm B)}(\omega,\Omega)]$ can be obtained explicitly as

$$\mathrm{Tr}\big[\tilde{\Lambda}_x^{(\rm A)}(\omega,\Omega)\big]=\sum_{\beta=0}^{3}\big\{\mathrm{Tr}\big[\tau_\beta\big[\tau_0+\tilde{\Lambda}_x^{(\rm A)}(\omega,\Omega)\big]\big]R_{{\rm A}1\beta}^{(x)}(\omega,\omega+\Omega)+\mathrm{Tr}\big[\tau_\beta\big[\tau_0+\tilde{\Lambda}_x^{(\rm B)}(\omega,\Omega)\big]\big]R_{{\rm B}1\beta}^{(x)}(\omega,\omega+\Omega)\big\}, \tag{A7a}$$

$$\mathrm{Tr}\big[\tilde{\Lambda}_x^{(\rm B)}(\omega,\Omega)\big]=\sum_{\beta=0}^{3}\big\{\mathrm{Tr}\big[\tau_\beta\big[\tau_0+\tilde{\Lambda}_x^{(\rm A)}(\omega,\Omega)\big]\big]R_{{\rm A}2\beta}^{(x)}(\omega,\omega+\Omega)+\mathrm{Tr}\big[\tau_\beta\big[\tau_0+\tilde{\Lambda}_x^{(\rm B)}(\omega,\Omega)\big]\big]R_{{\rm B}2\beta}^{(x)}(\omega,\omega+\Omega)\big\}, \tag{A7b}$$

respectively, with the functions

$$R_{{\rm A}1\beta}^{(x)}(\omega,\omega+\Omega)=\sum_{\gamma=0}^{3}C_{\rm A1}^{(x)}(\gamma)\tilde{I}_\gamma^{(\rm A)}(\beta,\omega,\omega+\Omega),\quad R_{{\rm A}2\beta}^{(x)}(\omega,\omega+\Omega)=\sum_{\gamma=0}^{3}C_{\rm A2}^{(x)}(\gamma)\tilde{I}_\gamma^{(\rm A)}(\beta,\omega,\omega+\Omega), \tag{A8a}$$

$$R_{{\rm B}1\beta}^{(x)}(\omega,\omega+\Omega)=\sum_{\gamma=0}^{3}C_{\rm B1}^{(x)}(\gamma)\tilde{I}_\gamma^{(\rm B)}(\beta,\omega,\omega+\Omega),\quad R_{{\rm B}2\beta}^{(x)}(\omega,\omega+\Omega)=\sum_{\gamma=0}^{3}C_{\rm B2}^{(x)}(\gamma)\tilde{I}_\gamma^{(\rm B)}(\beta,\omega,\omega+\Omega). \tag{A8b}$$

Now we turn to evaluate the similar traces of the product between the vertex kernel $\tilde{\Lambda}_x^{(\rm A)}(\omega,\Omega)$ and matrix τ_α with $\alpha=1,2,3$ in region A and the product of the vertex kernel $\tilde{\Lambda}_x^{(\rm B)}(\omega,\Omega)$ and matrix τ_α in region B in the kernel function (25), where the derivation processes are almost the same as the derivation processes for the above $\mathrm{Tr}[\tau_0\tilde{\Lambda}_x^{(\rm A)}(\omega,\Omega)]$ in Eq. (A7a) and

$\mathrm{Tr}[\tau_0\tilde{\Lambda}_x^{(\mathrm{B})}(\omega,\Omega)]$ in Eq. (A7b), and the obtained results can be expressed explicitly as

$$\mathrm{Tr}\big[\tau_\alpha\tilde{\Lambda}_x^{(\mathrm{A})}(\omega,\Omega)\big]=\sum_{\beta=0}^{3}\big\{\mathrm{Tr}\big[\tau_\beta\big[\tau_0+\tilde{\Lambda}_x^{(\mathrm{A})}(\omega,\Omega)\big]\big]R_{\mathrm{A}1\beta}^{(x)}(\alpha,\omega,\omega+\Omega)+\mathrm{Tr}\big[\tau_\beta\big[\tau_0+\tilde{\Lambda}_x^{(\mathrm{B})}(\omega,\Omega)\big]\big]R_{\mathrm{B}1\beta}^{(x)}(\alpha,\omega,\omega+\Omega)\big\}, \tag{A9a}$$

$$\mathrm{Tr}\big[\tau_\alpha\tilde{\Lambda}_x^{(\mathrm{B})}(\omega,\Omega)\big]=\sum_{\beta=0}^{3}\big\{\mathrm{Tr}\big[\tau_\beta\big[\tau_0+\tilde{\Lambda}_x^{(\mathrm{A})}(\omega,\Omega)\big]\big]R_{\mathrm{A}2\beta}^{(x)}(\alpha,\omega,\omega+\Omega)+\mathrm{Tr}\big[\tau_\beta\big[\tau_0+\tilde{\Lambda}_{(x)}^{(\mathrm{B})}(\omega,\Omega)\big]\big]R_{\mathrm{B}2\beta}^{(x)}(\alpha,\omega,\omega+\Omega)\big\}, \tag{A9b}$$

with the functions

$$R_{\mathrm{A}1\beta}^{(x)}(\alpha,\omega,\omega+\Omega)=\sum_{\lambda=0}^{3}C_{\mathrm{A}1\alpha}^{(x)}(\lambda)\tilde{I}_\lambda^{(\mathrm{A})}(\beta,\omega,\omega+\Omega), \tag{A10a}$$

$$\begin{aligned}C_{\mathrm{A}1\alpha}^{(x)}(\lambda)=n_iN\sum_{\mu,\nu=0}^{3}\left(\sum_\sigma i\bar{\epsilon}_{\mu\nu\sigma}i\bar{\epsilon}_{\sigma\alpha\lambda}\right)\eta_\alpha(\nu)\big[&T_{11}^{(\mu)}(\omega)T_{11}^{(\nu)}(\omega+\Omega)+T_{31}^{(\mu)}(\omega)T_{13}^{(\nu)}(\omega+\Omega)\\&-T_{51}^{(\mu)}(\omega)T_{15}^{(\nu)}(\omega+\Omega)-T_{71}^{(\mu)}(\omega)T_{17}^{(\nu)}(\omega+\Omega)\big],\end{aligned} \tag{A10b}$$

$$R_{\mathrm{B}1\beta}^{(x)}(\alpha,\omega,\omega+\Omega)=\sum_{\lambda=0}^{3}C_{\mathrm{B}1\alpha}^{(x)}(\lambda)\tilde{I}_\lambda^{(\mathrm{B})}(\beta,\omega,\omega+\Omega), \tag{A10c}$$

$$\begin{aligned}C_{\mathrm{B}1\alpha}^{(x)}(\lambda)=n_iN\tan\theta_{\mathrm{F}}\sum_{\mu,\nu=0}^{3}\left(\sum_\sigma i\bar{\epsilon}_{\mu\nu\sigma}i\bar{\epsilon}_{\sigma\alpha\lambda}\right)\eta_\alpha(\nu)\big[&T_{21}^{(\mu)}(\omega)T_{12}^{(\nu)}(\omega+\Omega)+T_{41}^{(\mu)}(\omega)T_{14}^{(\nu)}(\omega+\Omega)\\&-T_{61}^{(\mu)}(\omega)T_{16}^{(\nu)}(\omega+\Omega)-T_{81}^{(\mu)}(\omega)T_{18}^{(\nu)}(\omega+\Omega)\big],\end{aligned} \tag{A10d}$$

$$R_{\mathrm{A}2\beta}^{(x)}(\alpha,\omega,\omega+\Omega)=\sum_{\lambda=0}^{3}C_{\mathrm{A}2\alpha}^{(x)}(\lambda)\tilde{I}_\lambda^{(\mathrm{A})}(\beta,\omega,\omega+\Omega), \tag{A10e}$$

$$\begin{aligned}C_{\mathrm{A}2\alpha}^{(x)}(\lambda)=n_iN\cot\theta_{\mathrm{F}}\sum_{\mu,\nu=0}^{3}\left(\sum_\sigma i\bar{\epsilon}_{\mu\nu\sigma}i\bar{\epsilon}_{\sigma\alpha\lambda}\right)\eta_\alpha(\nu)\big[&T_{12}^{(\mu)}(\omega)T_{21}^{(\nu)}(\omega+\Omega)+T_{32}^{(\mu)}(\omega)T_{23}^{(\nu)}(\omega+\Omega)\\&-T_{52}^{(\mu)}(\omega)T_{25}^{(\nu)}(\omega+\Omega)-T_{72}^{(\mu)}(\omega)T_{27}^{(\nu)}(\omega+\Omega)\big],\end{aligned} \tag{A10f}$$

$$R_{\mathrm{B}2\beta}^{(x)}(\alpha,\omega,\omega+\Omega)=\sum_{\lambda=0}^{3}C_{\mathrm{B}2\alpha}^{(x)}(\lambda)\tilde{I}_\lambda^{(\mathrm{B})}(\beta,\omega,\omega+\Omega), \tag{A10g}$$

$$\begin{aligned}C_{\mathrm{B}2\alpha}^{(x)}(\lambda)=n_iN\sum_{\mu,\nu=0}^{3}\left(\sum_\sigma i\bar{\epsilon}_{\mu\nu\sigma}i\bar{\epsilon}_{\sigma\alpha\lambda}\right)\eta_\alpha(\nu)\big[&T_{22}^{(\mu)}(\omega)T_{22}^{(\nu)}(\omega+\Omega)+T_{42}^{(\mu)}(\omega)T_{24}^{(\nu)}(\omega+\Omega)\\&-T_{62}^{(\mu)}(\omega)T_{26}^{(\nu)}(\omega+\Omega)-T_{82}^{(\mu)}(\omega)T_{28}^{(\nu)}(\omega+\Omega)\big],\end{aligned} \tag{A10h}$$

where $\sum_\sigma i\bar{\epsilon}_{\mu\nu\sigma}i\bar{\epsilon}_{\sigma\alpha\lambda}$ satisfies the identity

$$\begin{aligned}\sum_\sigma i\bar{\epsilon}_{\mu\nu\sigma}i\bar{\epsilon}_{\sigma\alpha\lambda}=&-4\delta_{\mu0}\delta_{\nu0}\delta_{\alpha0}\delta_{\lambda0}+\delta_{\alpha\mu}\delta_{\lambda0}\delta_{\nu0}+\delta_{\alpha\nu}\delta_{\mu0}\delta_{\lambda0}+\delta_{\lambda\mu}\delta_{\nu0}\delta_{\alpha0}+\delta_{\mu0}\delta_{\alpha0}\delta_{\lambda\nu}+\delta_{\alpha\lambda}\delta_{\mu\nu}+\delta_{\alpha\nu}\delta_{\lambda\mu}-\delta_{\alpha\mu}\delta_{\lambda\nu}\\&+i\delta_{\alpha0}\epsilon_{\lambda\mu\nu}+i\delta_{\lambda0}\epsilon_{\alpha\mu\nu}+i\delta_{\mu0}\epsilon_{\nu\alpha\lambda}+i\delta_{\nu0}\epsilon_{\mu\alpha\lambda}\end{aligned} \tag{A11}$$

and the tensor $\eta_\alpha(\nu)$ is defined as

$$\eta_\alpha(\nu)=\begin{cases}1, & \nu=0,\alpha\\ -1, & \text{otherwise.}\end{cases} \tag{A12}$$

Substituting the above results from Eqs. (A7) and (A9) into Eq. (25) of the main text, we therefore obtain the kernel function $J_{xx}(\omega,\omega+\Omega)$ in Eq. (25) of the main text.

[1] J. R. Schrieffer, *Theory of Superconductivity* (Benjamin, New York, 1964).

[2] P. W. Anderson, Absence of diffusion in certain random lattices, Phys. Rev. **109**, 1492 (1958).

[3] D. N. Basov and T. Timusk, Infrared properties of high-T_c superconductors: An experimental overview, in *High-Temperature Superconductors - II*, Handbook on the Physics and Chemistry of Rare Earths, Vol. 31 (Elsevier, Amsterdam, 2001), Chap. 202, pp. 437–507.

[4] See, e.g., the review by N. E. Hussey, Low-energy quasiparticles in high-T_c cuprates, Adv. Phys. **51**, 1685 (2002).

[5] See, e.g., the review by A. V. Balatsky, I. Vekhter, and J.-X. Zhu, Impurity-induced states in conventional and unconventional superconductors, Rev. Mod. Phys. **78**, 373 (2006).

[6] See, e.g., the review by H. Alloul, J. Bobroff, M. Gabay, and P. J. Hirschfeld, Defects in correlated metals and superconductors, Rev. Mod. Phys. **81**, 45 (2009).

[7] See, e.g., the review by C. C. Tsuei and J. R. Kirtley, Pairing symmetry in cuprate superconductors, Rev. Mod. Phys. **72**, 969 (2000).

[8] K. Ishida, Y. Kitaoka, T. Yoshitomi, N. Ogata, T. Kamino, and K. Asayama, Gapless superconductivity in Zn-doped $YBa_2Cu_3O_7$ studied by Cu NMR and NQR: Possibility of d-wave superconductivity in high-T_c oxides, Physica C (Amsterdam) **179**, 29 (1991).

[9] A. Legris, F. Rullier-Albenque, E. Radeva, and P. Lejay, Effects of electron irradiation on $YBa_2Cu_3O_{7-\delta}$ superconductor, J. Phys. I **3**, 1605 (1993).

[10] J. Giapintzakis, D. M. Ginsberg, M. A. Kirk, and S. Ockers, Testing models of the symmetry of the superconducting pairing state by low-temperature electron irradiation of an untwinned single crystal of $YBa_2Cu_3O_{7-\delta}$, Phys. Rev. B **50**, 15967 (1994).

[11] Y. Fukuzumi, K. Mizuhashi, K. Takenaka, and S. Uchida, Universal Superconductor-Insulator Transition and T_c Depression in Zn-Substituted High-T_c Cuprates in the Underdoped Regime, Phys. Rev. Lett. **76**, 684 (1996).

[12] S. K. Tolpygo, J.-Y. Lin, M. Gurvitch, S. Y. Hou, and J. M. Phillips, Universal T_c suppression by in-plane defects in high-temperature superconductors: Implications for pairing symmetry, Phys. Rev. B **53**, 12454 (1996).

[13] J. P. Attfield, A. L. Kharlanov, and J. A. McAllister, Cation effects in doped La_2CuO_4 superconductors, Nature (London) **394**, 157 (1998).

[14] J. Bobroff, W. A. MacFarlane, H. Alloul, P. Mendels, N. Blanchard, G. Collin, and J.-F. Marucco, Spinless Impurities in High-T_c Cuprates: Kondo-Like Behavior, Phys. Rev. Lett. **83**, 4381 (1999).

[15] H. Eisaki, N. Kaneko, D. L. Feng, A. Damascelli, P. K. Mang, K. M. Shen, Z.-X. Shen, and M. Greven, Effect of chemical inhomogeneity in bismuth-based copper oxide superconductors, Phys. Rev. B **69**, 064512 (2004).

[16] D. A. Bonn, R. Liang, T. M. Riseman, D. J. Baar, D. C. Morgan, K. Zhang, P. Dosanjh, T. L. Duty, A. MacFarlane, G. D. Morris, J. H. Brewer, W. N. Hardy, C. Kallin, and A. J. Berlinsky, Microwave determination of the quasiparticle scattering time in $YBa_2Cu_3O_{6.95}$, Phys. Rev. B **47**, 11314 (1993).

[17] S.-F. Lee, D. C. Morgan, R. J. Ormeno, D. M. Broun, R. A. Doyle, J. R. Waldram, and K. Kadowaki, *a-b* Plane Microwave Surface Impedance of a High-Quality $Bi_2Sr_2CaCu_2O_8$ Single Crystal, Phys. Rev. Lett. **77**, 735 (1996).

[18] A. Hosseini, R. Harris, S. Kamal, P. Dosanjh, J. Preston, R. Liang, W. N. Hardy, and D. A. Bonn, Microwave spectroscopy of thermally excited quasiparticles in $YBa_2Cu_3O_{6.99}$, Phys. Rev. B **60**, 1349 (1999).

[19] P. J. Turner, R. Harris, S. Kamal, M. E. Hayden, D. M. Broun, D. C. Morgan, A. Hosseini, P. Dosanjh, G. K. Mullins, J. S. Preston, R. Liang, D. A. Bonn, and W. N. Hardy, Observation of Weak-Limit Quasiparticle Scattering via Broadband Microwave Spectroscopy of a d-Wave Superconductor, Phys. Rev. Lett. **90**, 237005 (2003).

[20] R. Harris, P. J. Turner, S. Kamal, A. R. Hosseini, P. Dosanjh, G. K. Mullins, J. S. Bobowski, C. P. Bidinosti, D. M. Broun, R. Liang, W. N. Hardy, and D. A. Bonn, Phenomenology of $\hat{a}$-axis and $\hat{b}$-axis charge dynamics from microwave spectroscopy of highly ordered $YBa_2Cu_3O_{6.50}$ and $YBa_2Cu_3O_{6.993}$, Phys. Rev. B **74**, 104508 (2006).

[21] D. A. Bonn, S. Kamal, K. Zhang, R. Liang, D. J. Baar, E. Klein, and W. N. Hardy, Comparison of the influence of Ni and Zn impurities on the electromagnetic properties of $YBa_2Cu_3O_{6.95}$, Phys. Rev. B **50**, 4051 (1994).

[22] C. Bucci, P. Carretta, R. D. Renzi, G. Guidia, F. Licci, L. G. Raflob, H. Keller, S. Lee, and I. M. Savićc, Penetration depth anisotropy in $YBa_2(Cu_{1-y}M_y)_3O_{7-x}$ (M=Zn.Ni) oriented powders by μSR, Physica C (Amsterdam) **235-240**, 1849 (1994).

[23] C. Bernhard, J. L. Tallon, C. Bucci, R. DeRenzi, G. Guidi, G. V. M. Williams, and C. Niedermayer, Suppression of the Superconducting Condensate in the High-T_c Cuprates by Zn Substitution and Overdoping: Evidence for an Unconventional Pairing State, Phys. Rev. Lett. **77**, 2304 (1996).

[24] J. Bobroff, Impurities and correlated systems. From chains to superconducting cuprates: Impurities and correlated systems, Ann. Phys. (Paris) **30**, 1 (2005).

[25] P. J. Hirschfeld, W. O. Putikka, and D. J. Scalapino, d-wave model for microwave response of high-T_c superconductors, Phys. Rev. B **50**, 10250 (1994).

[26] A. C. Durst and P. A. Lee, Impurity-induced quasiparticle transport and universal-limit Wiedemann-Franz violation in d-wave superconductors, Phys. Rev. B **62**, 1270 (2000).

[27] A. J. Berlinsky, D. A. Bonn, R. Harris, and C. Kallin, Microwave conductivity due to impurity scattering in a d-wave superconductor, Phys. Rev. B **61**, 9088 (2000).

[28] M. H. Hettler and P. J. Hirschfeld, Order-parameter holes and theory of microwave conductivity in $YBa_2Cu_3O_{7-\delta}$, Phys. Rev. B **61**, 11313 (2000).

[29] A. C. Durst and P. A. Lee, Microwave conductivity due to scattering from extended linear defects in d-wave superconductors, Phys. Rev. B **65**, 094501 (2002).

[30] W. Kim, F. Marsiglio, and J. P. Carbotte, Microwave conductivity of a high-purity d-wave superconductor, Phys. Rev. B **70**, 060505(R) (2004).

[31] T. S. Nunner and P. J. Hirschfeld, Microwave conductivity of d-wave superconductors with extended impurities, Phys. Rev. B **72**, 014514 (2005).

[32] Z. Wang, H. Guo, and S. Feng, Doping and energy dependent microwave conductivity of kinetic energy driven superconductors with extended impurities, Physica C (Amsterdam) **468**, 1078 (2008); Z. Wang and S. Feng, Anisotropic microwave conductivity of cuprate superconductors in the presence of CuO chain-induced impurities, Phys. Rev. B **80**, 174507 (2009).

[33] U. Chatterjee, M. Shi, A. Kaminski, A. Kanigel, H. M. Fretwell, K. Terashima, T. Takahashi, S. Rosenkranz, Z. Z. Li, H. Raffy, A. Santander-Syro, K. Kadowaki, M. R. Norman, M. Randeria, and J. C. Campuzano, Nondispersive Fermi Arcs and the Absence of Charge Ordering in the Pseudogap Phase of $Bi_2Sr_2CaCu_2O_{8+\delta}$, Phys. Rev. Lett. **96**, 107006 (2006).

[34] Y. He, Y. Yin, M. Zech, A. Soumyanarayanan, M. M. Yee, T. Williams, M. C. Boyer, K. Chatterjee, W. D. Wise, I. Zeljkovic, T. Kondo, T. Takeuchi, H. Ikuta, P. Mistark, R. S. Markiewicz, A. Bansil, S. Sachdev, E. W. Hudson, and J. E. Hoffman, Fermi surface and pseudogap evolution in a cuprate superconductor, Science **344**, 608 (2014).

[35] F. Restrepo, J. Zhao, J. C. Campuzano, and U. Chatterjee, Temperature and carrier concentration dependence of Fermi arcs in moderately underdoped $Bi_2Sr_2CaCu_2O_{8+\delta}$ cuprate high-temperature superconductors: A joint density of states perspective, Phys. Rev. B **107**, 174519 (2023).

[36] M. R. Norman, H. Ding, M. Randeria, J. C. Campuzano, T. Yokoya, T. Takeuchi, T. Takahashi, T. Mochiku, K. Kadowaki, P. Guptasarma, and D. G. Hinks, Destruction of the Fermi surface in underdoped high-T_c superconductors, Nature (London) **392**, 157 (1998).

[37] M. Shi, J. Chang, S. Pailhés, M. R. Norman, J. C. Campuzano, M. Mánsson, T. Claesson, O. Tjernberg, A. Bendounan, L. Patthey, N. Momono, M. Oda, M. Ido, C. Mudry, and J. Mesot, Coherent d-Wave Superconducting Gap in Underdoped $La_{2-x}Sr_xCuO_4$ by Angle-Resolved Photoemission Spectroscopy, Phys. Rev. Lett. **101**, 047002 (2008).

[38] Y. Sassa, M. Radović, M. Mánsson, E. Razzoli, X. Y. Cui, S. Pailhés, S. Guerrero, M. Shi, P. R. Willmott, F. Miletto Granozio, J. Mesot, M. R. Norman, and L. Patthey, Ortho-II band folding in $YBa_2Cu_3O_{7-\delta}$ films revealed by angle-resolved photoemission, Phys. Rev. B **83**, 140511(R) (2011).

[39] K. Fujita, C. K. Kim, I. Lee, J. Lee, M. H. Hamidian, I. A. Firmo, S. Mukhopadhyay, H. Eisaki, S. Uchida, M. J. Lawler, E.-A. Kim, and J. C. Davis, Simultaneous transitions in cuprate momentum-space topology and electronic symmetry breaking, Science **344**, 612 (2014).

[40] R. Comin, A. Frano, M. M. Yee, Y. Yoshida, H. Eisaki, E. Schierle, E. Weschke, R. Sutarto, F. He, A. Soumyanarayanan, Y. He, M. L. Tacon, I. S. Elfimov, J. E. Hoffman, G. A. Sawatzky, B. Keimer, and A. Damascelli, Charge order driven by Fermi-arc instability in $Bi_2Sr_{2-x}La_xCuO_{6+\delta}$, Science **343**, 390 (2014).

[41] A. Kaminski, T. Kondo, T. Takeuchi, and G. Gu, Pairing, pseudogap and Fermi arcs in cuprates, Philos. Mag. **95**, 453 (2015).

[42] B. Loret, S. Sakai, S. Benhabib, Y. Gallais, M. Cazayous, M. A. Méasson, R. D. Zhong, J. Schneeloch, G. D. Gu, A. Forget, D. Colson, I. Paul, M. Civelli, and A. Sacuto, Vertical temperature boundary of the pseudogap under the superconducting dome in the phase diagram of $Bi_2Sr_2CaCu_2O_{8+\delta}$, Phys. Rev. B **96**, 094525 (2017).

[43] S. D. Chen, M. Hashimoto, Y. He, D. Song, K. J. Xu, J. F. He, T. P. Devereaux, H. Eisaki, D. H. Lu, J. Zaanen, and Z.-X. Shen, Incoherent strange metal sharply bounded by a critical doping in Bi2212, Science **366**, 1099 (2019).

[44] See, e.g., the review by J.-X. Yin, S. H. Pan, and M. Z. Hasan, Probing topological quantum matter with scanning tunnelling microscopy, Nat. Rev. Phys. **3**, 249 (2021).

[45] S. H. Pan, J. P. O'Neal, R. L. Badzey, C. Chamon, H. Ding, J. R. Engelbrecht, Z. Wang, H. Eisaki, S. Uchida, A. K. Gupta, K.-W. Ng, E. W. Hudson, K. M. Lang, and J. C. Davis, Microscopic electronic inhomogeneity in the high-T_c superconductor $Bi_2Sr_2CaCu_2O_{8+x}$, Nature (London) **413**, 282 (2001).

[46] Y. Kohsaka, C. Taylor, K. Fujita, A. Schmidt, C. Lupien, T. Hanaguri, M. Azuma, M. Takano, H. Eisaki, H. Takagi, S. Uchida, and J. C. Davis, An intrinsic bond-centered electronic glass with unidirectional domains in underdoped cuprates, Science **315**, 1380 (2007).

[47] Y. Kohsaka, C. Taylor, P. Wahl, A. Schmidt, J. Lee, K. Fujita, J. W. Alldredge, K. McElroy, J. Lee, H. Eisaki, S. Uchida, D.-H. Lee, and J. C. Davis, How Cooper pairs vanish approaching the Mott insulator in $Bi_2Sr_2CaCu_2O_{8+x}$, Nature (London) **454**, 1072 (2008).

[48] M. H. Hamidian, S. D. Edkins, S. Hyun Joo, A. Kostin, H. Eisaki, S. Uchida, M. J. Lawler, E.-A. Kim, A. P. Mackenzie, K. Fujita, J. Lee, and J. C. S. Davis, Detection of a Cooper-pair density wave in $Bi_2Sr_2CaCu_2O_{8+x}$, Nature (London) **532**, 343 (2016).

[49] S. Feng, Kinetic energy driven superconductivity in doped cuprates, Phys. Rev. B **68**, 184501 (2003); S. Feng, T. Ma, and H. Guo, Magnetic nature of superconductivity in doped cuprates, Physica C (Amsterdam) **436**, 14 (2006).

[50] S. Feng, H. Zhao, and Z. Huang, Two gaps with one energy scale in cuprate superconductors, Phys. Rev. B **85**, 054509 (2012); Publisher's Note: Two gaps with one energy scale in cuprate superconductors [Phys. Rev. B 85, 054509 (2012)], **85**, 099902 (2012).

[51] See, e.g., the review by S. Feng, Y. Lan, H. Zhao, L. Kuang, L. Qin, and X. Ma, Kinetic energy driven superconductivity in cuprate superconductors, Int. J. Mod. Phys. B **29**, 1530009 (2015).

[52] S. Feng, L. Kuang, and H. Zhao, Electronic structure of cuprate superconductors in a full charge-spin recombination scheme, Physica C (Amsterdam) **517**, 5 (2015); Z. Cao, Y. Liu, H. Guo, and S. Feng, Enhancement of superconductivity by electronic nematicity in cuprate superconductors, Philos. Mag. **102**, 918 (2022).

[53] M. Zeng, X. Li, Y. Wang, and S. Feng, Influence of impurities on the electronic structure in cuprate superconductors, Phys. Rev. B **106**, 054512 (2022).

[54] P. W. Anderson, The resonating valence bond state in La_2CuO_4 and superconductivity, Science **235**, 1196 (1987).

[55] F. C. Zhang and T. M. Rice, Effective Hamiltonian for the superconducting Cu oxides, Phys. Rev. B **37**, 3759 (1988).

[56] See, e.g., the review by Y. Lu, Many-body problems in high temperature superconductivity, in *Recent Progress in Many-Body Theories*, edited by T. L. Ainsworth, C. E. Campbell, B. E. Clements, and E. Krotscheck (Plenum, New York, 1992), Vol. 3, pp. 157–181.

[57] S. Feng, J. B. Wu, Z. B. Su, and L. Yu, Slave-particle studies of the electron-momentum distribution in the low-dimensional t-J model, Phys. Rev. B **47**, 15192 (1993).

[58] L. Zhang, J. K. Jain, and V. J. Emery, Importance of the local constraint in slave-boson theories, Phys. Rev. B **47**, 3368 (1993).

[59] J. C. LeGuillou and E. Ragoucy, Slave-particle quantization and sum rules in the t-J model, Phys. Rev. B **52**, 2403 (1995).

[60] S. Feng, J. Qin, and T. Ma, A gauge invariant dressed holon and spinon description of the normal state of underdoped cuprates, J. Phys.: Condens. Matter **16**, 343 (2004); S. Feng, Z. B. Su, and L. Yu, Fermion-spin transformation to implement the charge-spin separation, Phys. Rev. B **49**, 2368 (1994).

[61] Y. Liu, Y. Lan, and S. Feng, Peak structure in the self-energy of cuprate superconductors, Phys. Rev. B **103**, 024525 (2021).

[62] D. Gao, Y. Liu, H. Zhao, Y. Mou, and S. Feng, Interplay between charge order and superconductivity in cuprate superconductors, Physica C (Amsterdam) **551**, 72 (2018).

[63] D. Gao, Y. Mou, Y. Liu, S. Tan, and S. Feng, Autocorrelation of quasiparticle spectral intensities and its connection with quasiparticle scattering interference in cuprate superconductors, Philos. Mag. **99**, 752 (2019).

[64] See, e.g., G. D. Mahan, *Many-Particle Physics* (Plenum, New York, 1981).

[65] P. J. Hirschfeld, P. Wölfle, J. A. Sauls, D. Einzel, and W. O. Putikka, Electromagnetic absorption in anisotropic superconductors, Phys. Rev. B **40**, 6695 (1989).

[66] P. J. Hirschfeld and N. Goldenfeld, Effect of strong scattering on the low-temperature penetration depth of a d-wave superconductor, Phys. Rev. B **48**, 4219(R) (1993).

[67] D. S. Dessau, B. O. Wells, Z.-X. Shen, W. E. Spicer, A. J. Arko, R. S. List, D. B. Mitzi, and A. Kapitulnik, Anomalous Spectral Weight Transfer at the Superconducting Transition of $Bi_2Sr_2CaCu_2O_{8+\delta}$, Phys. Rev. Lett. **66**, 2160 (1991).

[68] Y. Hwu, L. Lozzi, M. Marsi, S. LaRosa, M. Winokur, P. Davis, M. Onellion, H. Berger, F. Gozzo, F. Lévy, and G. Margaritondo, Electronic Spectrum of the High-Temperature Superconducting State, Phys. Rev. Lett. **67**, 2573 (1991).

[69] M. Randeria, H. Ding, J.-C. Campuzano, A. Bellman, G. Jennings, T. Yokoya, T. Takahashi, H. Katayama-Yoshida, T. Mochiku, and K. Kadowaki, Momentum Distribution Sum Rule for Angle-Resolved Photoemission, Phys. Rev. Lett. **74**, 4951 (1995).

[70] A. V. Fedorov, T. Valla, P. D. Johnson, Q. Li, G. D. Gu, and N. Koshizuka, Temperature Dependent Photoemission Studies of Optimally Doped $Bi_2Sr_2CaCu_2O_8$, Phys. Rev. Lett. **82**, 2179 (1999).

[71] D. H. Lu, D. L. Feng, N. P. Armitage, K. M. Shen, A. Damascelli, C. Kim, F. Ronning, Z.-X. Shen, D. A. Bonn, R. Liang, W. N. Hardy, A. I. Rykov, and S. Tajima, Superconducting Gap and Strong In-Plane Anisotropy in Untwinned $YBa_2Cu_3O_{7-\delta}$, Phys. Rev. Lett. **86**, 4370 (2001).

[72] S. Sakai, S. Blanc, M. Civelli, Y. Gallais, M. Cazayous, M.-A. Méasson, J. S. Wen, Z. J. Xu, G. D. Gu, G. Sangiovanni, Y. Motome, K. Held, A. Sacuto, A. Georges, and M. Imada, Raman-Scattering Measurements and Theory of the Energy-Momentum Spectrum for Underdoped $Bi_2Sr_2CaCu_2O_{8+\delta}$ Superconductors: Evidence of an s-Wave Structure for the Pseudogap, Phys. Rev. Lett. **111**, 107001 (2013).

[73] D. Mou, A. Kaminski, and G. Gu, Direct observation of self-energy signatures of the resonant collective mode in $Bi_2Sr_2CaCu_2O_{8+\delta}$, Phys. Rev. B **95**, 174501 (2017).